VA-092-053-TR

SERDP PROJECT CU-1121 ANNUAL REPORT FOR 1999

PROCESSING TECHNIQUES FOR DISCRIMINATION BETWEEN BURIED UXO AND CLUTTER USING MULTISENSOR ARRAY DATA

PERFORMING ORGANIZATIONS

AETC INC.
1225 Jefferson Davis Hwy Suite 800
Arlington, VA 22202

GEOPHEX LTD.
605 Mercury St.
Raleigh, NC 27603

VIEWS, OPINIONS, AND/OR FINDINGS CONTAINED IN THIS REPORT ARE THOSE OF THE AUTHOR(S) AND SHOULD NOT BE CONSTRUED AS AN OFFICIAL DEPARTMENT OF THE ARMY POSITION, POLICY, OR DECISION, UNLESS SO DESIGNATED BY OTHER OFFICIAL DOCUMENTATION.

AETC *Incorporated*
1225 JEFFERSON DAVIS HIGHWAY, SUITE 800
ARLINGTON, VA 22202

20000720 146

DTIC QUALITY INSPECTED 4

REPORT DOCUMENTATION PAGE

Public reporting burden for this collection of information is estimated to average 1 hour per response, including the time for reviewing instructions, searching existing data sources, gathering and maintaining the data needed, and completing and reviewing this collection of information. Send comments regarding this burden estimate or any other aspect of this collection of information, including suggestions for reducing this burden to Washington Headquarters Services, Directorate for Information Operations and Reports, 1215 Jefferson Davis Highway, Suite 1204, Arlington, VA 22202-4302, and to the Office of Management and Budget, Paperwork Reduction Project (0704-0188), Washington, DC 20503

1. AGENCY USE ONLY (Leave blank)	2. REPORT DATE 1999	3. REPORT TYPE AND DATES COVERED Annual Report

4. TITLE AND SUBTITLE
Processing Techniques for Discrimination Between Buried UXO and Clutter Using Multisensor Array Data

5. FUNDING NUMBERS
N/A

6. AUTHOR(S)
J. Miller, B. Barrow, T. Bell, D. Keiswetter, and I.J. Won

7. PERFORMING ORGANIZATION NAME(S) AND ADDRESS(ES)

AETC INC.
1225 Jefferson Davis Hwy Suite 800
Arlington, VA 22202

GEOPHEX LTD.
605 Mercury St.
Raleigh, NC 27603

8. PERFORMING ORGANIZATION REPORT NUMBER
N/A

9. SPONSORING / MONITORING AGENCY NAME(S) AND ADDRESS(ES)
SERDP
901 North Stuart St. Suite 303
Arlington, VA 22203

10. SPONSORING / MONITORING AGENCY REPORT NUMBER
N/A

11. SUPPLEMENTARY NOTES
No copyright is asserted in the United States under Title 17, U.S. code. The U.S. Government has a royalty-free license to exercise all rights under the copyright claimed herein for Government purposes. All other rights are reserved by the copyright owner.

12a. DISTRIBUTION / AVAILABILITY STATEMENT
Approved for public release: distribution is unlimited.

12b. DISTRIBUTION CODE
A

13. ABSTRACT *(Maximum 200 Words)*

The overall objective of this project is to develop reliable techniques for discriminating between buried UXO and clutter using multisensor elecrromagnetic induction sensor array data. The basic idea is to build on existing research which exploits differences in shape between ordnance and clutter to include the effects of other distinctive properties of ordnance items (fuze bodies, driving bands, fin assemblies, etc.). During the course of this project, we will clearly elucidate the underlying physical principles relating to the electromegnetic response of ordnance items, determine the fundamental physical limitations on ordnance/clutter discrimination using multisensor survey data, and devise effective multisensor processing schemes to discriminate between buried UXO and clutter using such data.

14. SUBJECT TERMS
SERDP, SERDP Collection, UXO, multisensor array data, clutter, electromagnetic induction sensor

15. NUMBER OF PAGES
65

16. PRICE CODE
N/A

17. SECURITY CLASSIFICATION OF REPORT	18. SECURITY CLASSIFICATION OF THIS PAGE	19. SECURITY CLASSIFICATION OF ABSTRACT	20. LIMITATION OF ABSTRACT
unclass	unclass	unclass	UL

NSN 7540-01-280-5500

Standard Form 298 (Rev. 2-89)
Prescribed by ANSI Std. Z39-18
298-102

TABLE OF CONTENTS

PROJECT BACKGROUND

This project addresses the issue of discriminating between buried unexploded ordnance (UXO) and clutter in the context of environmental cleanup. In spite of the recent advances in UXO detection performance, false alarms due to clutter (signals incorrectly diagnosed as having been caused by UXO) remain a serious problem. With traditional survey methods, the Army Corps of Engineers finds that 85-95% of all detected targets are not UXO. Since the cost of identifying and disposing of UXO in the United States using current technologies is estimated to range up to $500 billion, increases in performance efficiency due to reduced false alarm rates can result in substantial cost savings.

Typical ordnance items have certain distinctive attributes that distinguish them from clutter. They have a characteristic shape (long and slender) and their composition is distinctive (typically comprising a steel body with a brass or aluminum fuze body and copper driving bands or an aluminum fin assembly). Our experience, described in detail below, is that these attributes correspond to distinctive signatures in magnetic and electromagnetic induction sensor data. Current research activities are directed towards exploiting differences in shape between ordnance and clutter with commercially available sensors. This project is aimed at systematically exploring the performance improvements which are realized when additional distinguishing target attributes are included in the discrimination process.

OBJECTIVE

The overall objective of this project is to develop reliable techniques for discriminating between buried UXO and clutter using multisensor electromagnetic induction sensor array data. The basic idea is to build on existing research which exploits differences in shape between ordnance and clutter to include the effects of other distinctive properties of ordnance items (fuze bodies, driving bands, fin assemblies, etc.). During the course of this project, we will clearly elucidate the underlying physical principles relating to the electromagnetic response of ordnance items, determine the fundamental physical limitations on ordnance/clutter discrimination using

multisensor survey data, and devise effective multisensor processing schemes to discriminate between buried UXO and clutter using such data.

Annual objectives for the first year yielded results which may be useful to the UXO community in their own right, separate from carrying our work toward the overall project goal. One such objective was to collect a large body of data on UXO objects, clutter, and other test objects (spheres and cylinders), and to organize the data into an easily accessible database, which is now available for download from the SERDP ftp site. Another such objective was to systematically evaluate field performance of the GEM-3 sensor, including analysis of the information content in EMI signals available for target discrimination, amid contribution from competing signal sources under field conditions. These results were published at the SERDP symposium December 2, 1999. Annual objectives for next year involve development of efficient models to describe EMI response, which are necessary for inverting data and discriminating targets. The final project objective will draw on all these results to provide reliable algorithms for UXO discrimination.

TECHNICAL APPROACH

The technical approach that will be used to attain the objectives consists of five major elements, shown in table 1.

1	Fully characterize ordnance electromagnetic induction (EMI) spectra.
2	Determine appropriate basis functions and implement them in UXO signature models
3	Develop parameter estimation procedures for fitting UXO signal models to multi-axis spectra
4	Assemble a clutter signature library
5	Establish decision rules for UXO/clutter discrimination and evaluate their performance.

Table 1. The overall technical approach consists of five major elements.

Ordnance signature characterization is based on the magnetic polarizability tensor determined from measurements of the induced dipole moment with different target orientations. We will determine the complex eigenvalues of the polarizability tensor as a function of frequency from 30 Hz to 24 kHz. The primary technical issues here are the effects of eddy currents in the ground and range-dependent nondipole signature contributions. In developing ordnance signature models, we will decompose the polarizability tensor into a basic response that depends only on the ratio of size to skin depth, permeability and aspect ratio, and a residual response that includes the effects of body shape and constituent elements. The major technical difficulty will be in expressing the residual response as a sum of basis functions. These may be simple model forms (sphere, ring, plate), measured signatures of constituent parts (fins, fuzes, rotating bands, etc.), or if necessary empirical functions and coupling relationships determined using genetic programming techniques. There are two stages in the parameter estimation process for fitting UXO signal models to measured EMI spectra: first, the coordinate rotation needed to diagonalize the response must be determined, then the UXO model must be matched to the response matrix. We will develop modified steepest descent techniques for determining the coordinate rotations

2

and fitting models to data. If conventional gradient search techniques prove inadequate, we will resort to genetic algorithm and/or genetic programming techniques to introduce evolving functions for representing inductive coupling effects not explicitly included in the models. The clutter signature library will be used in establishing decision rules for UXO/clutter discrimination and in evaluating their performance. It will be based on measurements of EMI spectra for a large number of representative clutter items recovered in excavations at various sites including several Native American Lands (Badlands Bombing Range, Laguna Pueblo, Walker River, etc.) and the DARPA clutter sites (Ft. A. P. Hill and Ft. Carson). Finally, we will establish decision rules for UXO/clutter discrimination and evaluate their performance. Classification of an observation as UXO or clutter will be based on a target feature vector that includes estimated model parameters and the goodness of fit between the UXO model and the data. We will use a linear discriminant function for the decision rule. The linear discriminant measures the statistical separation of the data from UXO and clutter distributions. A large number of UXO and clutter signature measurements will be needed to estimate population statistics. Performance will be measured by the receiver operating characteristic (ROC), which represents the probability of detection vs. the probability of false alarm as the threshold or operating point is varied.

PROJECT ACCOMPLISHMENTS

1) Executive Summary of Reported Findings

This summary gives a brief description of progress in the first year, with references to publications where our results have been made available. A following section gives more detail and covers results which were not included in the publications referenced here.

One of our first tasks was to determine how well the GEM-3 sensor could reproduce analytical results for spheres. This information would be needed to validate the instrument and as a starting point for developing models of EMI response for general objects. After overcoming some problems with the GEM-3, we were able to get very good agreement with analytic solutions. These results will appear in two papers presented this year at SAGEEP '00 (appendicies A and B).

Having validated sensor accuracy, we then measured EMI response for a wide range of objects including UXO, spheres, cylinders, and clutter. We compiled more than 100,000 individual measurements, representing each object at several distances, orientations, and conditions and all these data are now available in a Microsoft Access database at the SERDP ftp site (AETC, 1999).

We needed to address a crucial go/no-go question this year, namely; is there enough information in EMI data for effective discrimination of UXO? The answer required careful evaluation of signal distortions due to competing effects such as presence of conducting ground, changing depth, non-uniform material properties of the object, and target surface condition. We found that target-specific features can be found which are stronger by an order of magnitude than any competing effect. So our conclusion is "yes", there is ample data available for effective discrimination. These findings were published in a poster presentation at the SERDP

Symposium '99 (appendix C) and will be presented again in papers submitted to SPIE '00 (appendix D), SPIE SSTA '00 (appendix E) and IGARSS '00 (appendix F).

A major goal for the first year was to develop a baseline model for EMI response of arbitrarily shaped conducting objects. We succeeded in doing so, and the resulting 3-parameter model fits a wide range of objects surprisingly well. The model will be presented in a paper at SAGEEP '00 (appendix G).

We observed a consistent pattern of response for cylinders of differing sizes, but common length-to-diameter aspect ratio (2:1, 4:1, and 8:1 aspect ratios were tested). By concatenating graphs for cylinders with common aspect ratio, we developed "type curves" to describe this pattern. These type curves help validate the appropriateness of our baseline model and provide insight for objects of similar aspect ratio. This result was described in an oral presentation at the SERDP Symposium '99 (appendix H).

Analysis of the data revealed that driving bands, the soft metal rings near the tail of a projectile designed to make sliding contact with the gun bore, are responsible for a large artifact in the overall response of many projectiles. This fact offers a promising tool for target discrimination since driving bands are only found on UXO. These results are described in a paper accepted for presentation at the UXO/Countermine Forum '00 (appendix I).

2) Accomplishment Details

This section provides more detail on our accomplishments in general, and describes results not included in the publications referenced in the previous section. Considerable progress has been made in the first year. Four tasks were identified in the execution plan for 1999, listed in table 2, all of which have been successfully completed.

Task	Status
1.1 Measure and analyze UXO and baseline spectra	Complete
1.2 Determine ground and competing effects	Complete
1.3 Develop a baseline model	Complete
1.4 Evaluate UXO signature content	Complete

Table 2. Project tasks for 1999 have been completed.

2a) Overcoming problems with the GEM-3 instrument

The GEM-3 sensor manufactured by Geophex Ltd. is being used in this project (Figure 1). The GEM-3 employs a pair of concentric circular coils to generate the primary magnetic field, and current runs in opposite directions in these coils thereby setting up a zone of magnetic cavity at the center where the primary field strength approaches zero. A third receiving coil is placed within this magnetic cavity so that it senses only the weak secondary field resulting from eddy currents in the buried target. All coils are molded into a single circular disk in a fixed geometry

and precisely known dimensions. The instrument is being used in frequency domain mode, and measurements are made at several frequencies ranging from 30Hz to 24kHz. A more detailed description of the GEM-3 may be found in appendix B.
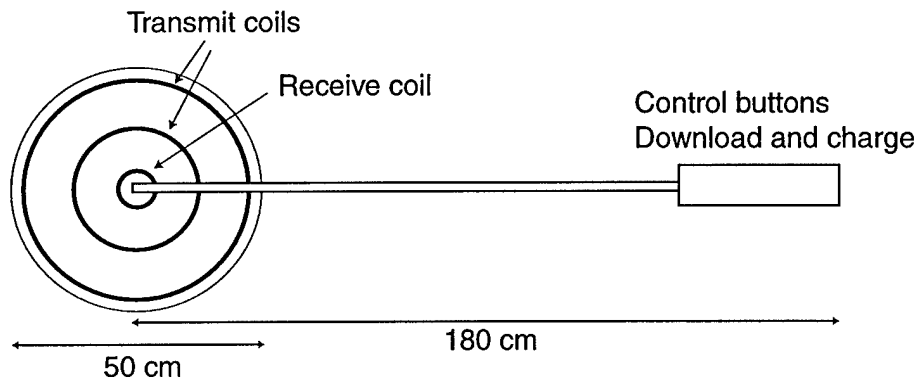
Figure 1. Top view (plan) of the GEM-3 instrument.

Data from the GEM-3 initially showed some problems. We observed significant fluctuations in measurement toward the higher frequencies which were erratic and not repeatable from one run to another. The in-phase signal would sometimes decrease with increasing frequency, which is not physically possible, so we knew it had to be a problem with the instrument. We traced the problem to fluctuations in the background signal, and solved it by taking background measurements more frequently and interpolating between them. This provided a much better estimation of the true background level present during the moment when the measurement on the target object was made. The problem was eliminated. New versions of the GEM-3 have built-in temperature probes to address the background drift problem.

Another problem came to light when we looked at data from ferrite rods. Ferrite has a well known EMI response, characterized by zero quadrature and a strong in-phase component that remains constant over the entire range of frequencies measured by the GEM-3, from 0 to 30 kHz. This is due to the fact that ferrite is a non-conductor so eddy currents cannot easily develop at the surface to cancel out the field inside the object. Measurements on ferrite rods with the GEM-3 were found to have non-constant behavior with frequency, revealing an error in the phase and amplitude of the signal. The error was measured and corrected using customized software applied to the data. (Figure 2).
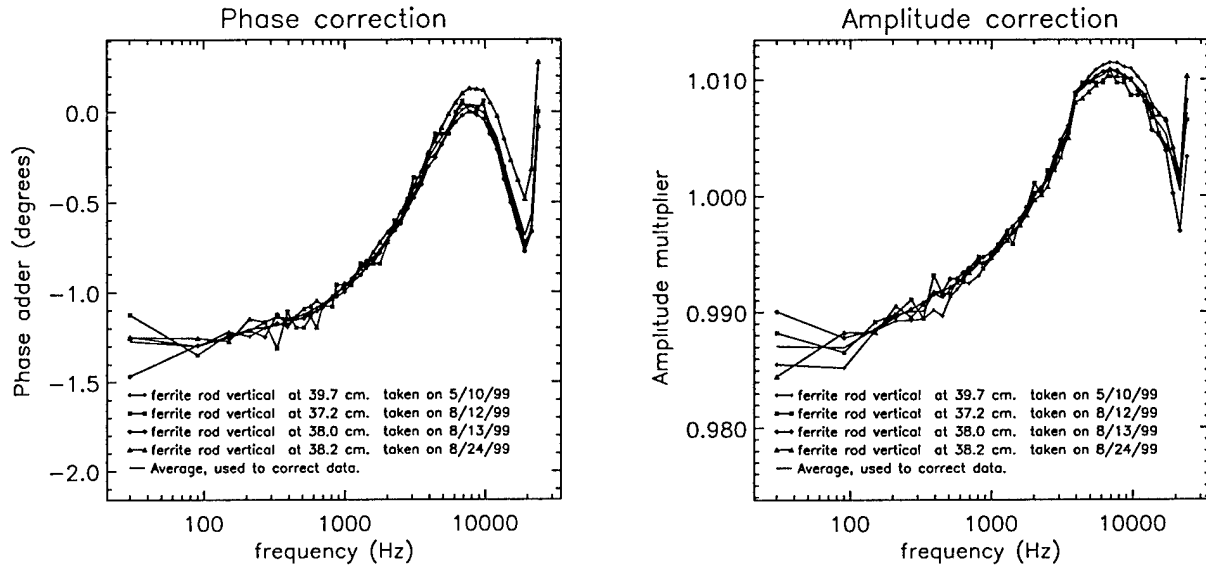
Phase correction

Amplitude correction

Figure 2. Phase and amplitude corrections for GEM-3 data are determined from measurements on ferrite rods.

After applying these corrections, very good agreement was achieved between GEM-3 measurements on steel spheres and the analytical models (figure 3), giving confirmation that the instrument is working properly. A more detailed description of the sphere model fit to GEM-3 data will be presented at SAGEEP '00 this year (appendix A), and these results also appear in another paper to be presented at SAGEEP '00 (appendix B).
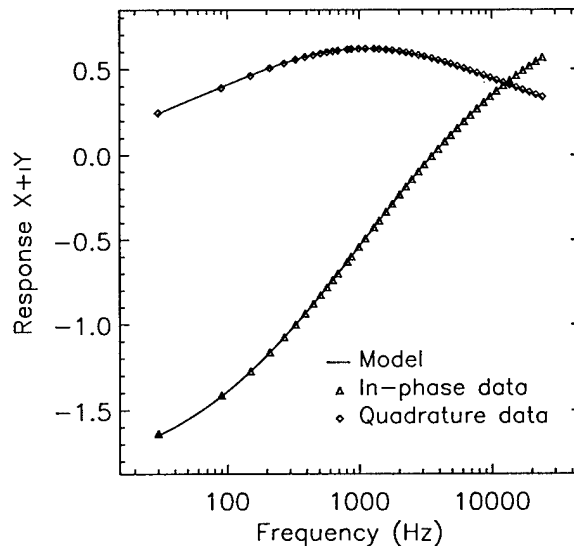
Figure 3. Analytical model for spheres fit to GEM-3 data measured on a 3 inch diameter chrome steel ball. The match is within 1% overall, and within 1/10 of a percent above about 1 kHz where the signal-to-noise ratio is better. Details of this fit can be found in appendix A.

2b) Collecting test data and assembling a database

A large set of EMI data was collected on a variety of test objects under controlled conditions. The GEM-3 was suspended in an all-wooden frame and distances and angles were carefully recorded (Figure 4).
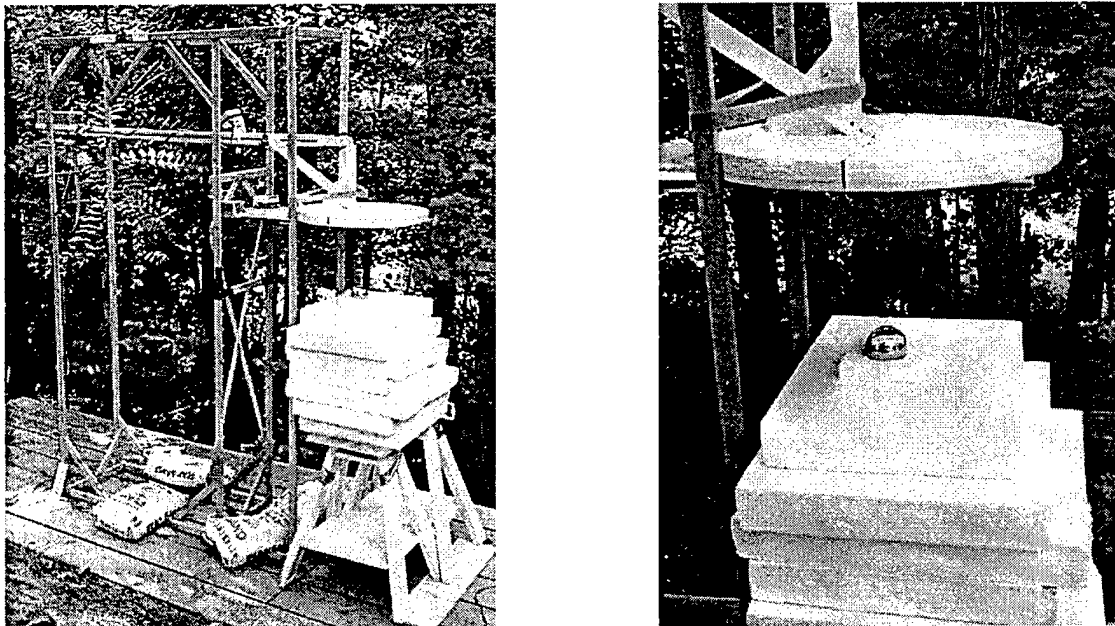

Figure 4. The GEM-3 instrument was set up to measure test objects under controlled conditions. These pictures show a 3-inch diameter steel ball being tested.

More than 100,000 individual measurements were taken on a variety of test objects (Figure 5), over a range of distances and orientations. All the data has been organized into a Microsoft Access database (AETC, 1999) which includes EMI response, object dimensions, shape, composition, orientation, and all relevant distances. Background measurements and measurements on wire coils and ferrite rods are also included to allow proper calibration of the instrument. A querying tool is included that searches through all the data tables to find data for a given object. Another tool is also provided in the database which downloads all data to text files so they can be read normally by other software.
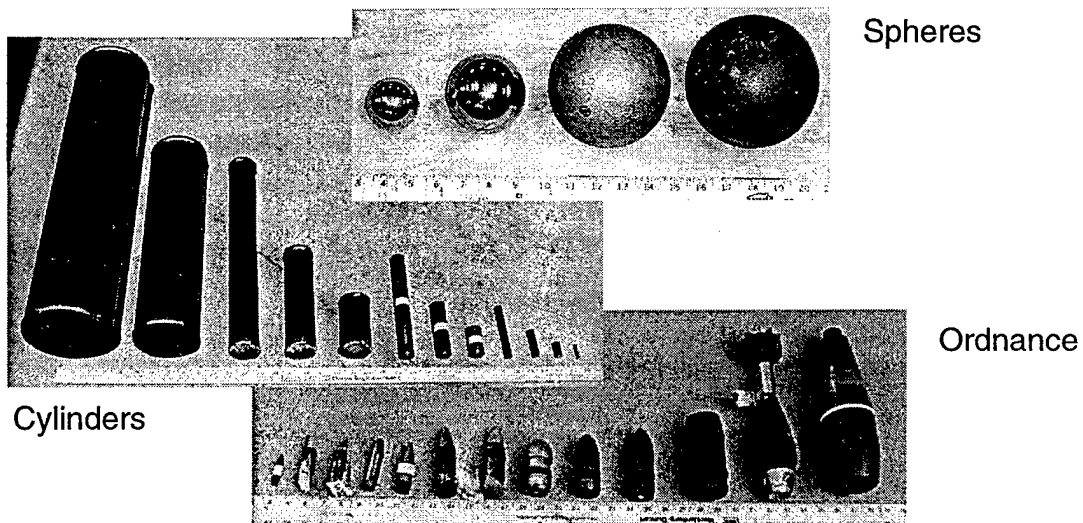
7

Figure 5. A variety of test objects were measured to investigate the capabilities of the GEM-3 and to provide a basis for analysis.

2c) Evaluation of information content in EMI

Having seen some data, we needed to answer a crucial go/no-go question, namely; is there enough information in these data for effective discrimination of UXO? This involved careful evaluation of signal distortions due to competing effects such as presence of conducting ground, changing depth, non-uniform material properties of the object, and target surface condition. Figure 6 shows our evaluation for the case of ground effects.
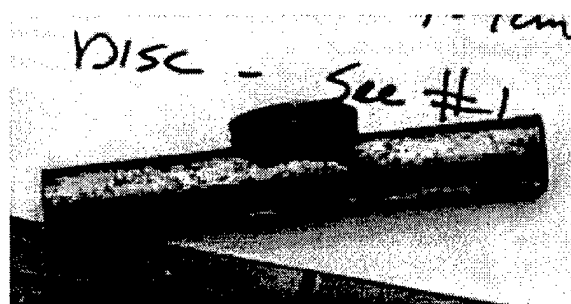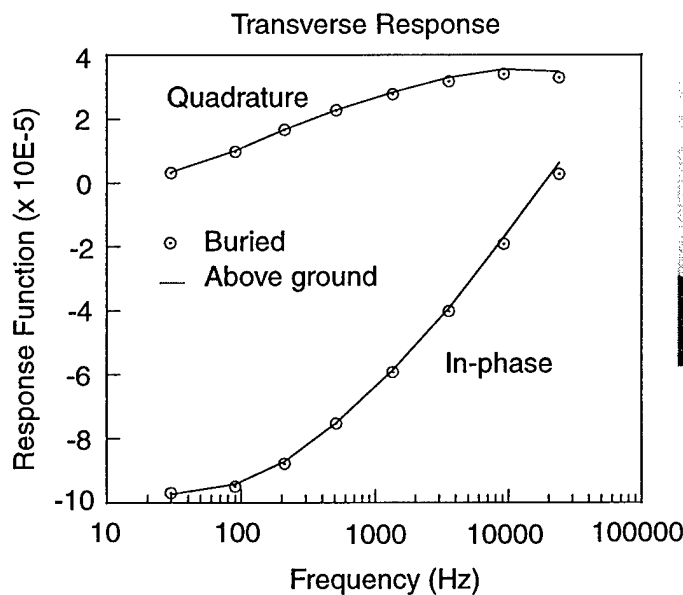
Small clutter object measured in ground and above ground.

Figure 6. The influence of conducting soil around the object was determined to be less than 5%. This was one of five effects investigated.

8

We evaluated five likely sources of signal distortion and determined that under worst case, the most severe effect would cause about 6% distortion in the signal (table 3). At the same time, we determined that target-specific features can be found which are stronger by an order of magnitude than any of these competing effects (figure 7). So our conclusion is "yes", there is ample data available for effective discrimination. These findings were published in a poster presentation at the 1999 SERDP Symposium (appendix C) and will also appear in three upcoming conferences (appendicies D, E, and F).

Conducting ground effects	< 5%
Depth effects	Up to ~6% for large objects.
Inhomogeneous material composition	< 1%
Target surface (rust, paint)	< 1%
Temperature (over a range of ~30 °C)	< 1%

Table 3. Several effects which could potentially interfere with UXO discrimination were evaluated.
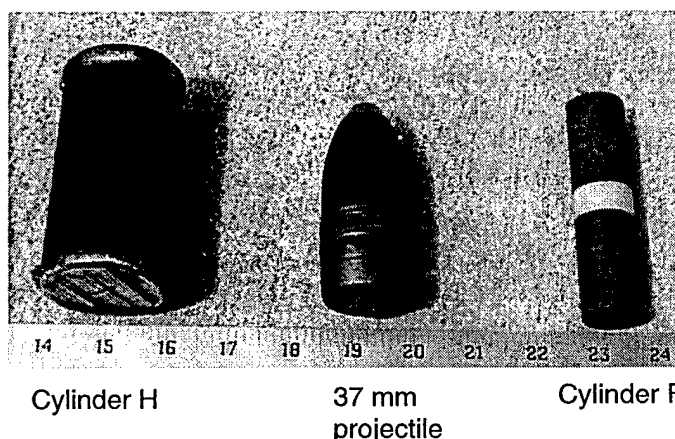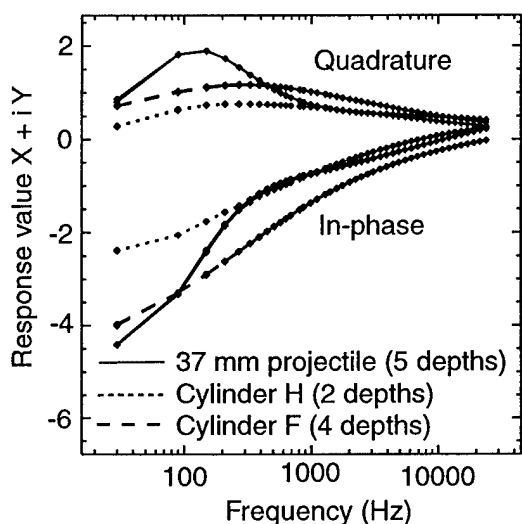
Figure 7. EMI response from the 37mm projectile shows strong differences from response of similarly sized cylinders. This difference is consistent over a range of depths, and it is about an order of magnitude larger than any competing effect.

2d) The baseline model

A general model based on the analytic solutions for spheres and horizontal infinite cylinders has been developed, which fits a wide variety of objects surprisingly well. This model stems from the observation that for high values of relative permeability, the sphere model S, and horizontal infinite cylinder model C, appear to be very similar (figure 8).

9

Sphere model (Grant and West 1965)

Horizontal infinite cylinder model (Ward and Hohman 1987)

Figure 8. Analytic models for a sphere S and a horizontal infinite cylinder C show striking similarities.

In fact, for high values of relative permeability, the models can be related by a simple transform, so that they overlap completely (Figure 9).
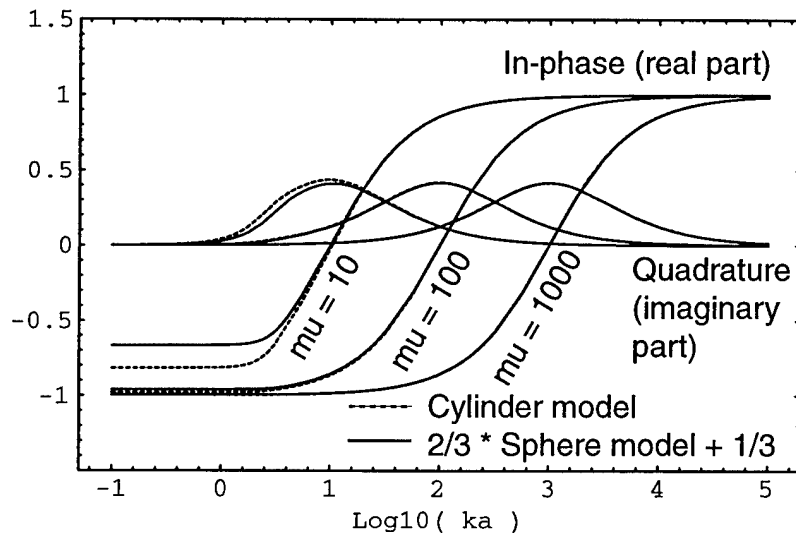
Figure 9. For objects with relative permeability greater than about 100, the analytical models for a sphere S and a horizontal infinite cylinder C can be related by a simple transform: $C = 2/3 \; S \; + 1/2$.

The general baseline model G is patterned after this relationship:
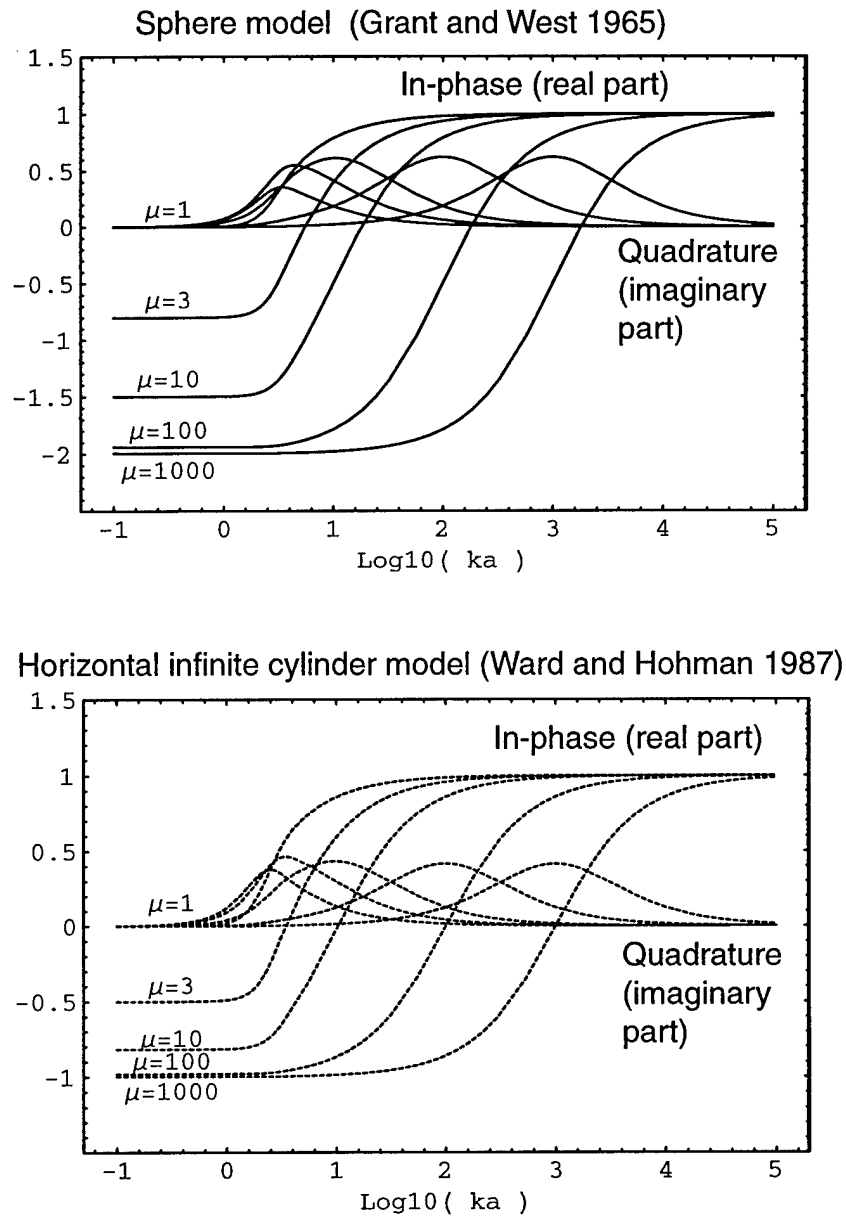
$$G = a\,S + b,$$

where parameters a and b are derived from asymptotic response values at high and low frequencies. These asymptotic values depend on relative permeability μ and demagnetization factor n of the object, as given in (Bell et. al. 1998). Response at low frequency R_L and high frequency R_H are

$$R_L = -\frac{2}{3}\frac{(\mu-1)}{(1+(\mu-1)n)} \quad , \text{and}$$

$$R_H = -\frac{2}{3}\frac{1}{(1-n)}.$$

Term a is found by setting a = (desired range of response)/(sphere model range):

$$a(\mu,n) = \frac{R_H(n) - R_L(\mu,n)}{1 - R_L(\mu,\frac{1}{3})} \qquad \text{Note that } n = 1/3 \text{ for the case of a sphere.}$$

$$= \frac{-2(\mu+2)}{9(n-1)(1+(\mu-1)n)}.$$

Term b is found by setting b = (desired high frequency value) – (current high frequency value)

11

$$b(\mu,n) = R_H(n) - a(\mu,n) = \frac{-2(\mu-1)(3n-1)}{9(n-1)(1+(\mu-1)n)}$$

This model has 3 parameters: permeability (μ), conductivity (σ), and demagnetization factor (n), each of which has physical meaning which can be compared to published values. Demagnetization factors for right circular cylinders are available from (Moskowitz et. al. 1966) and shown in figure 10.

Demagnetization factors for right circular cylinders.
Curve fit to published data from Moskowitz et. al. 1966
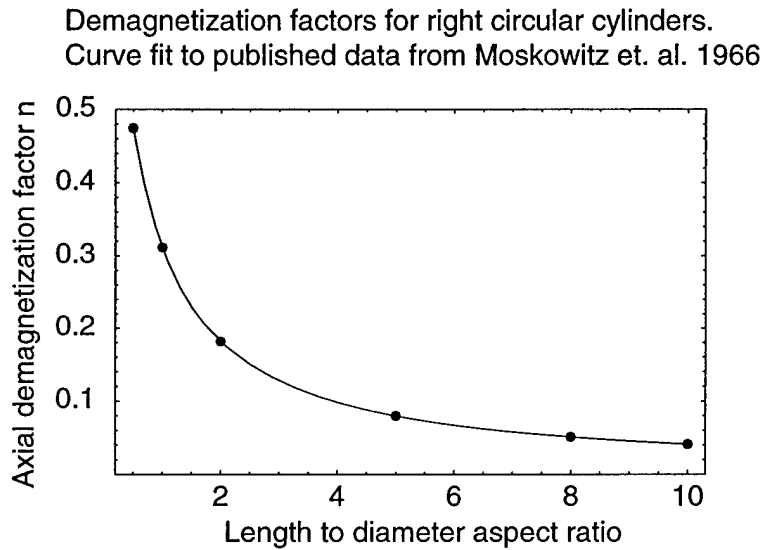
Figure 10. Published values of axial demagnetization factors can be used for model parameters.

This model fits a wide variety of objects including certain ordnance items and non-ordnance items surprisingly well. Fitted parameters agree reasonably well with expected values in most cases. In some cases the model fit to the data may be good but fitted parameters are not physically realistic. We have determined that model parameters may be insensitive under certain regimes (large objects with high permeability), leading to large and un-physical adjustments by the automatic calibration routine. Our evaluation and refinement of this model are ongoing. We are also working on ways to systematically analyze the residuals (model – data) in order to extract additional shape information about the target.

2e) Effects of skin depth

Analysis of EMI response from cylinders revealed artifacts originating from the interaction of skin depth to wall thickness of hollow objects (figure 11).

12
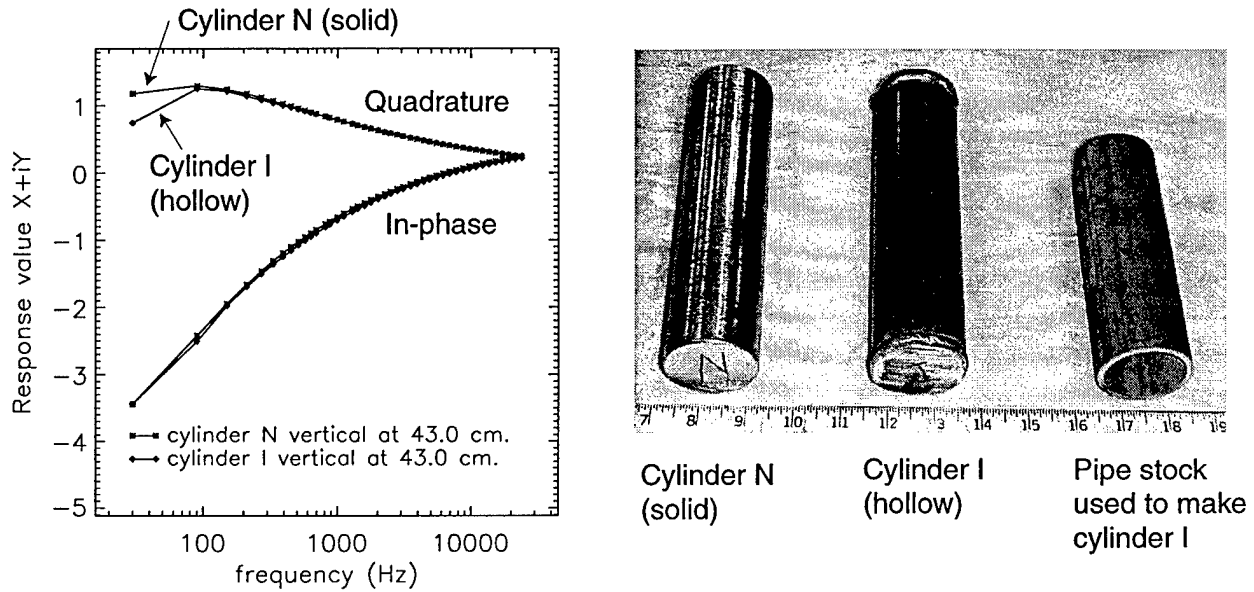
Figure 11. Differences in EMI response arose when the skin depth approached the wall thickness of the hollow cylinder.

Skin depth (δ) is the distance at which the magnetic field has attenuated by a factor of 1/e, found from the formula

$$\delta = \sqrt{\frac{2}{\sigma\mu\omega}} \quad ,$$

which is a function of conductivity (σ), permeability (μ), and frequency (ω). Assuming typical values for steel of $\sigma = 1E7$ (mho/m) and $\mu = 20 * \mu_0 = 20 * 4\pi$ E-7 (N/Amp^2), we calculate skin depth at 100 Hz, the point where the curves diverge, to be 3.6 mm. This agrees well with the actual wall thickness of 3.2 mm for cylinder I.

2f) Type curves for cylinders of uniform aspect ratio

We found a consistent pattern of response for cylinders of arbitrary size, but common length-to-diameter aspect ratio (2:1, 4:1, and 8:1 were tested). By concatenating graphs for different sized cylinders but identical aspect ratio, we developed "type curves" to describe this pattern, providing insight for further refinement of our models (Figure 12). These curves are plotted vs. dimensionless plot parameter ka which is defined from permeability (μ), conductivity (σ), angular frequency (ω), and a characteristic length (a), which was equal to the cylinder diameter in this case.

$$ka = a\sqrt{i\sigma\mu\omega} \quad .$$

13
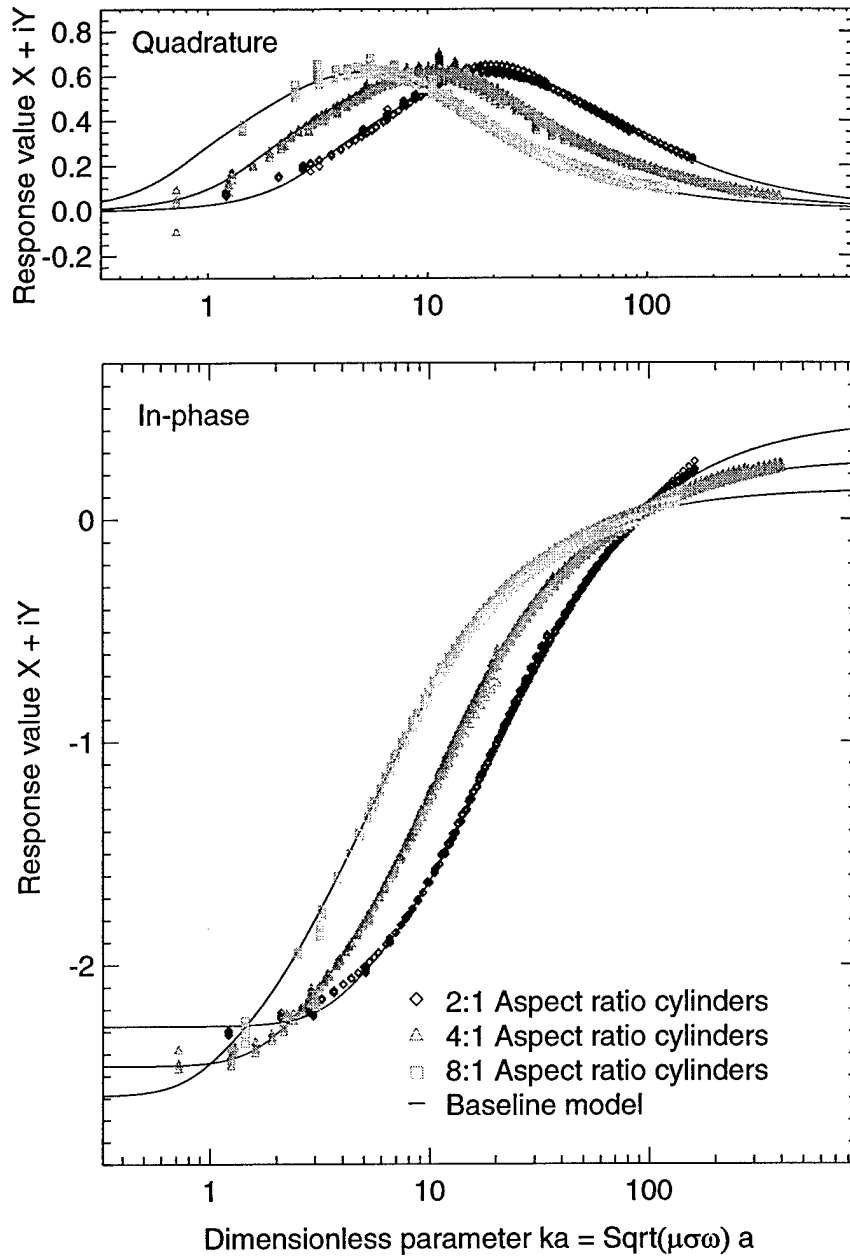
Figure 12. Type curves for cylinders of constant length-to-diameter aspect ratio match data.

2g) Effects due to shape

Figures 13 through 15 show residuals (baseline model – data) for the case of a cylinder with and without a small point cut into one end. These observations show no measureable change in EMI signal due to the point.

14

In-phase residuals for cylinder M over 9 sweeps.
Max depth= 78. cm. Min depth= 25. cm.

Mu = 20 for all 9 sweeps (not allowed to vary)
sigma was allowed to vary individually for each sweep. Fitted
values ranged from 9.07e7 to 10.8e7.

Quadrature residuals for cylinder M over 9 sweeps.
Max depth= 78. cm. Min depth= 25. cm.

Cylinder M is
2 by 8 inch
solid steel.
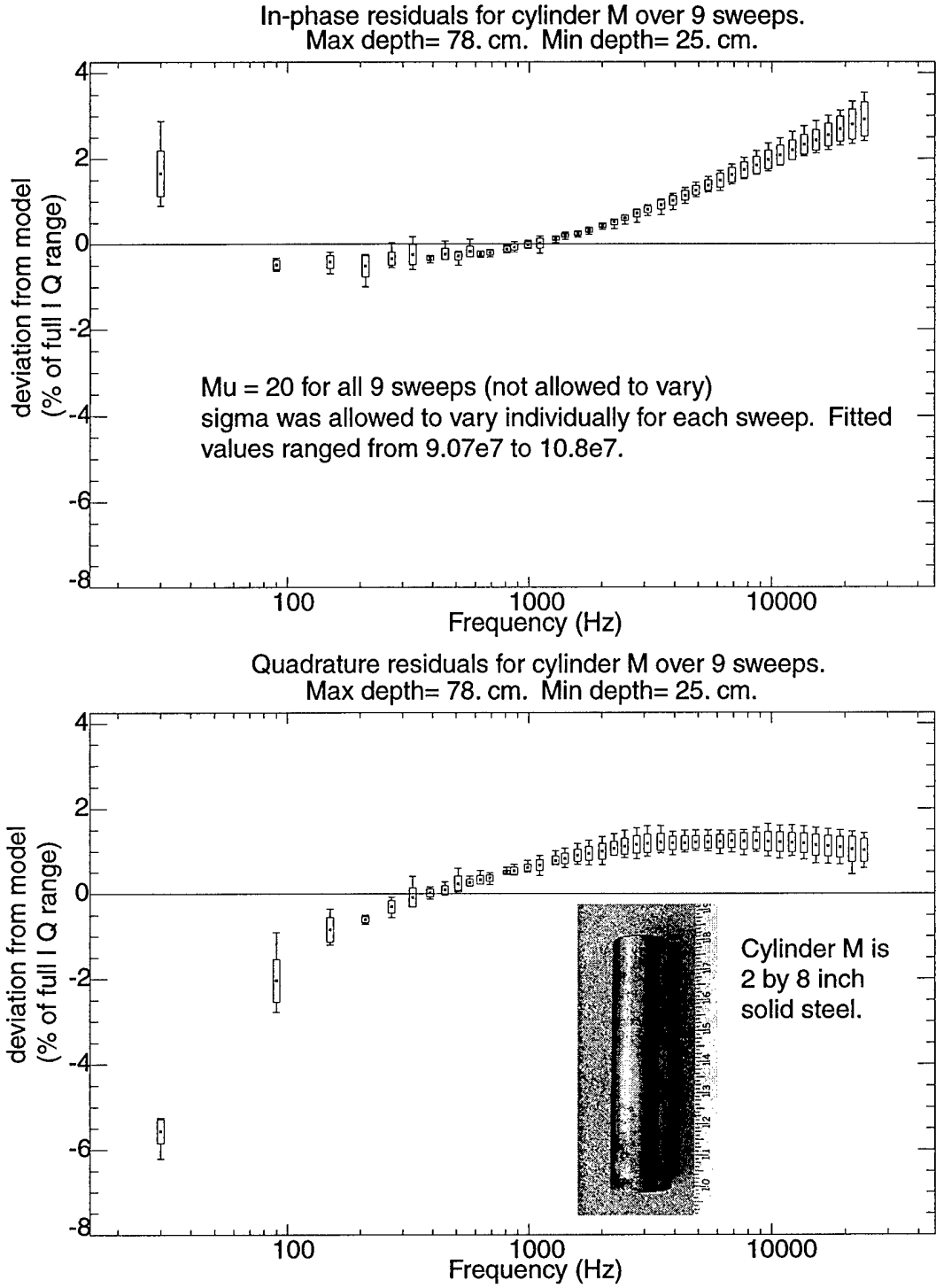
Figure 13. Residuals (model – data) for right circular cylinder M.

15

In-phase residuals for cylinder N over 7 sweeps.
Max depth= 78. cm. Min depth= 32. cm.

Mu = 20 for all 9 sweeps (not allowed to vary)
sigma was allowed to vary individually for each sweep. Fitted
values ranged from 8.31e7 to 9.44e7.

Quadrature residuals for cylinder N over 7 sweeps.
Max depth= 78. cm. Min depth= 32. cm.

Cylinder N is
2 by 8 inch
solid steel with
a point cut
into one end.
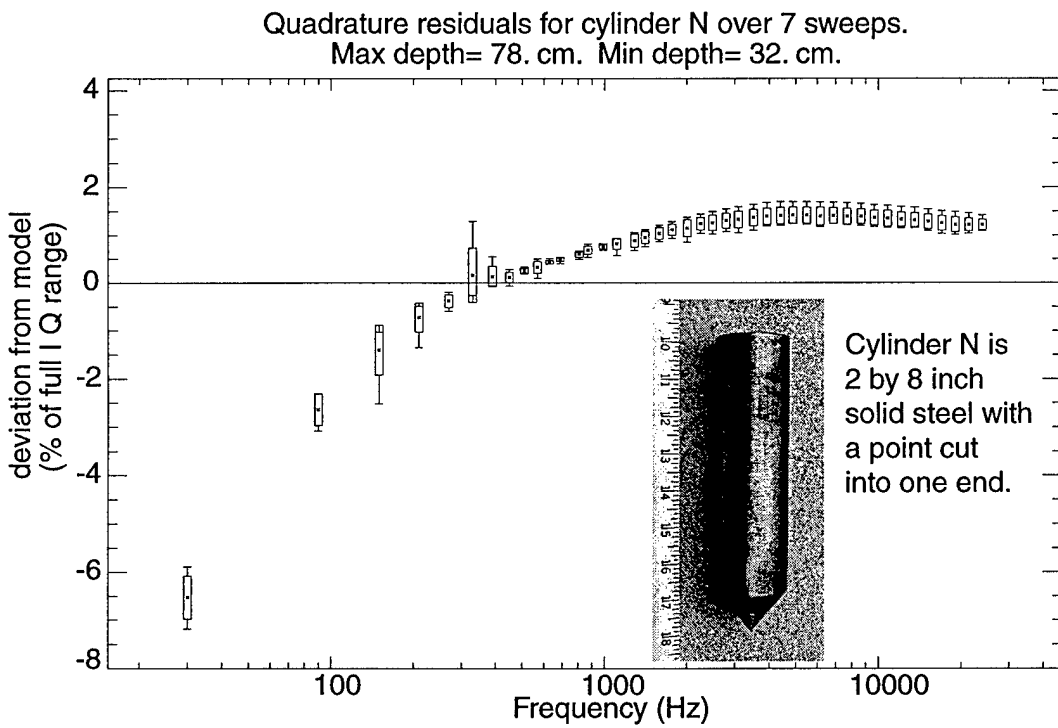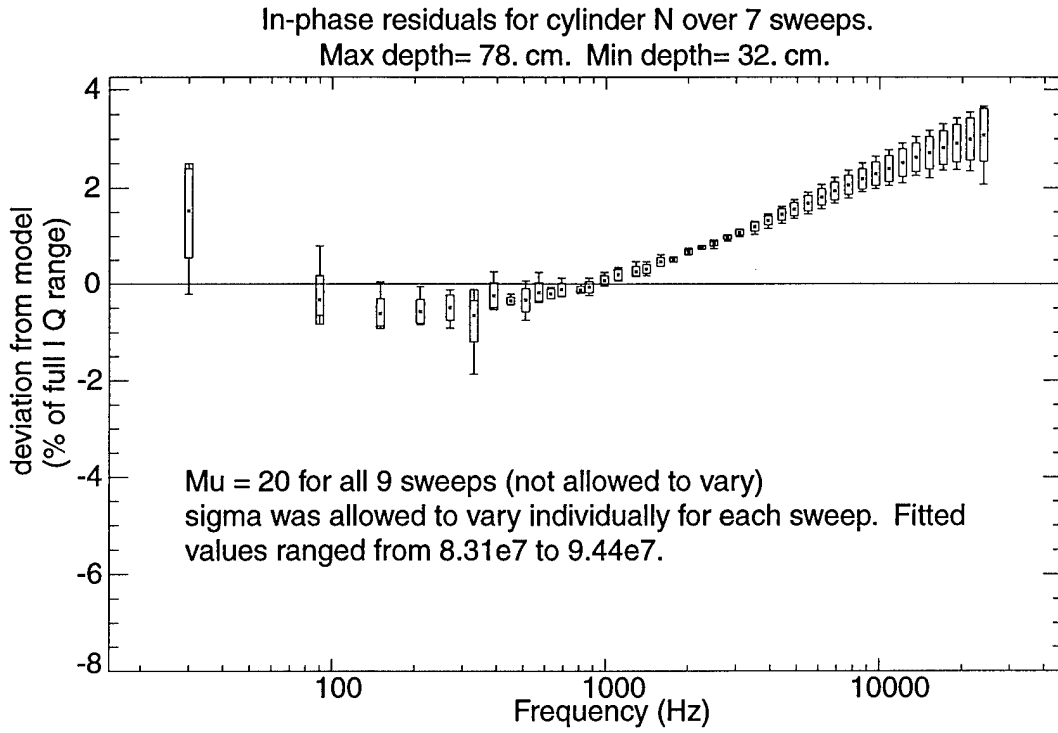
Figure 14. Residuals (model – data) for cylinder N nose down.

In-phase residuals for cylinder N over 7 sweeps.
Max depth= 78. cm. Min depth= 32. cm.

Mu = 20 for all 9 sweeps (not allowed to vary)
sigma was allowed to vary individually for each sweep. Fitted
values ranged from 7.42e7 to 8.86e7.

Quadrature residuals for cylinder N over 7 sweeps.
Max depth= 78. cm. Min depth= 32. cm.

Cylinder N is
2 by 8 inch
solid steel with
a point cut
into one end.
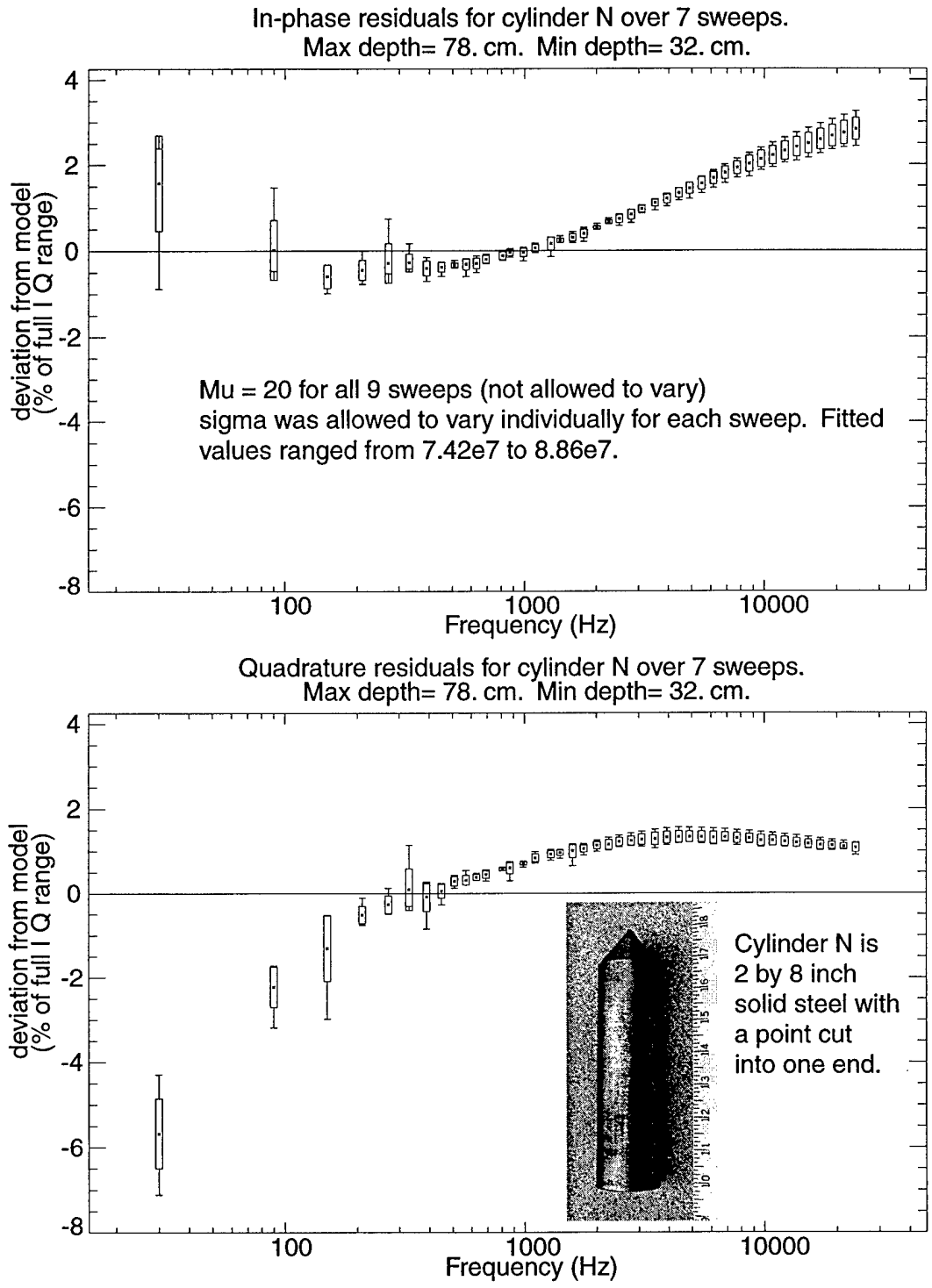
Figure 15. Residuals (model − data) for cylinder N nose up.

When the preceding figures are compared, the error bars all overlap, indicating we have no statistical difference in EMI response of these shapes and therefore no chance to discriminate between them. This represents a limitation of the technology; for objects with subtle variations in shape such as these, EMI is not going to be capable of resolving differences under field

17

conditions. However, other features of typical UXO produce very strong EMI response, which appear to be promising for discrimination, as described in the following section.

2h) Effect of a driving band

Driving bands are soft metal rings near the tail of a projectile designed to make sliding contact with rifling grooves in the gun bore when the projectile is fired. They are typically made of copper and found on a wide variety of projectile types and sizes. We have been able to produce EMI signals very similar to that from a projectile with a driving band, using a steel pin with a copper loop around it (Figure 16). The contribution from the copper loop was assessed independently by measuring components separately. We found that the copper loop alone produces a relatively weak response, but when when placed around the steel pin, it produces a strong feature in the overall EMI response which is particularly easy to detect and identify. This feature is characterized by a relatively sharp peak in quadrature similar to the response of a wire loop alone. We attribute this signal to a combination of three factors: 1) the relatively high conductivity of the copper loop compared with the body of the object, 2) the fact that the copper is in the shape of a loop, and 3) the capability of wide-band EMI instruments to sweep a range of frequencies, ensuring excitation of the frequencies where the contribution from the loop is strong.

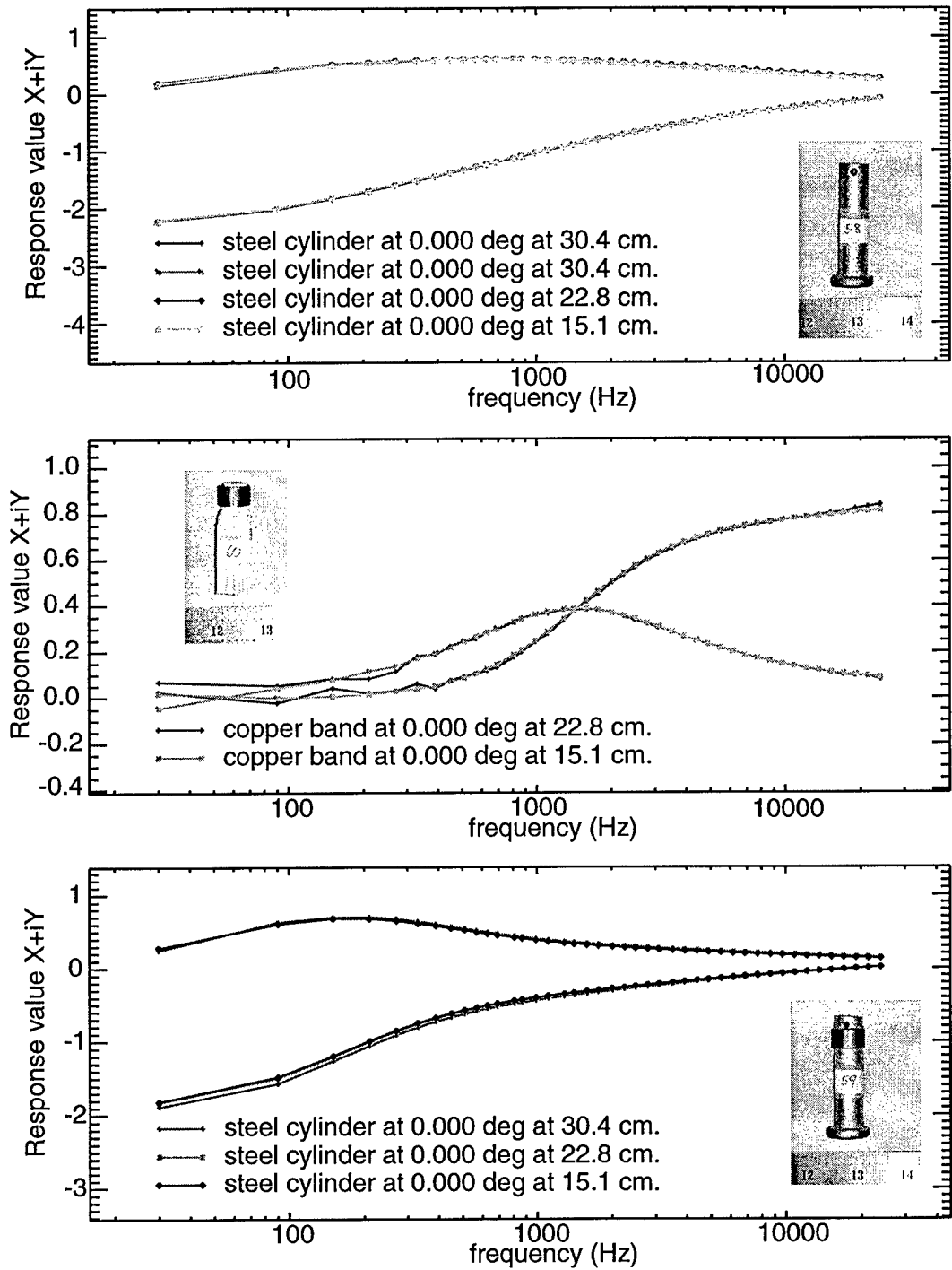Figure 16. The presence of a copper band around the steel pin causes a dramatic change in response. Note that we are evaluating *shape* of the response in these graphs, and amplitudes have been normalized. Actual magnitudes of response vary with distance and type of target object. In particular, the copper loop alone produces a relatively weak signal compared to it's influence when it interacts with the steel pin.

Figure 16 shows a strong effect when the copper band is present, very similar to the response of a 37mm projectile with driving band, shown previously in figure 7. This suggests the copper driving band on the projectile is causing the characteristic shape of the response. More experiments are underway to confirm this. The artifact due to the copper band is strong enough to be useful in target discrimination. In addition, the location of the peak in the quadrature curve is related to the size of the copper loop, leading to the possibility that the projectile caliber may also be determined from this artifact.

2i) Effect of ferrous content

The contribution of ferrous material to the overall EMI response is complicated. Figure 17 shows that when ferrite is introduced inside a copper cylinder, the overall signal is strongly altered. At high frequency, the copper pipe/ferrite rod combination behaves like a copper pipe alone, as expected since eddy currents at the copper surface cancel out all magnetic fields inside the object. At low frequency, we expect the copper pipe/ferrite rod combination to behave like the ferrite rod alone, since the magnetic field penetrates through the copper without interference. The figure suggests this is occurring, but the frequency range does not go low enough to confirm it positively. Somewhat more puzzling is the fact that introduction of the ferrite rod apparently moves the quadrature peak to the left, which is opposite the direction expected based on the analytic models. In the analytic models for the sphere and cylinder, an increase in relative permeability causes the quadrature peak to shift to the right. We are currently studying this.
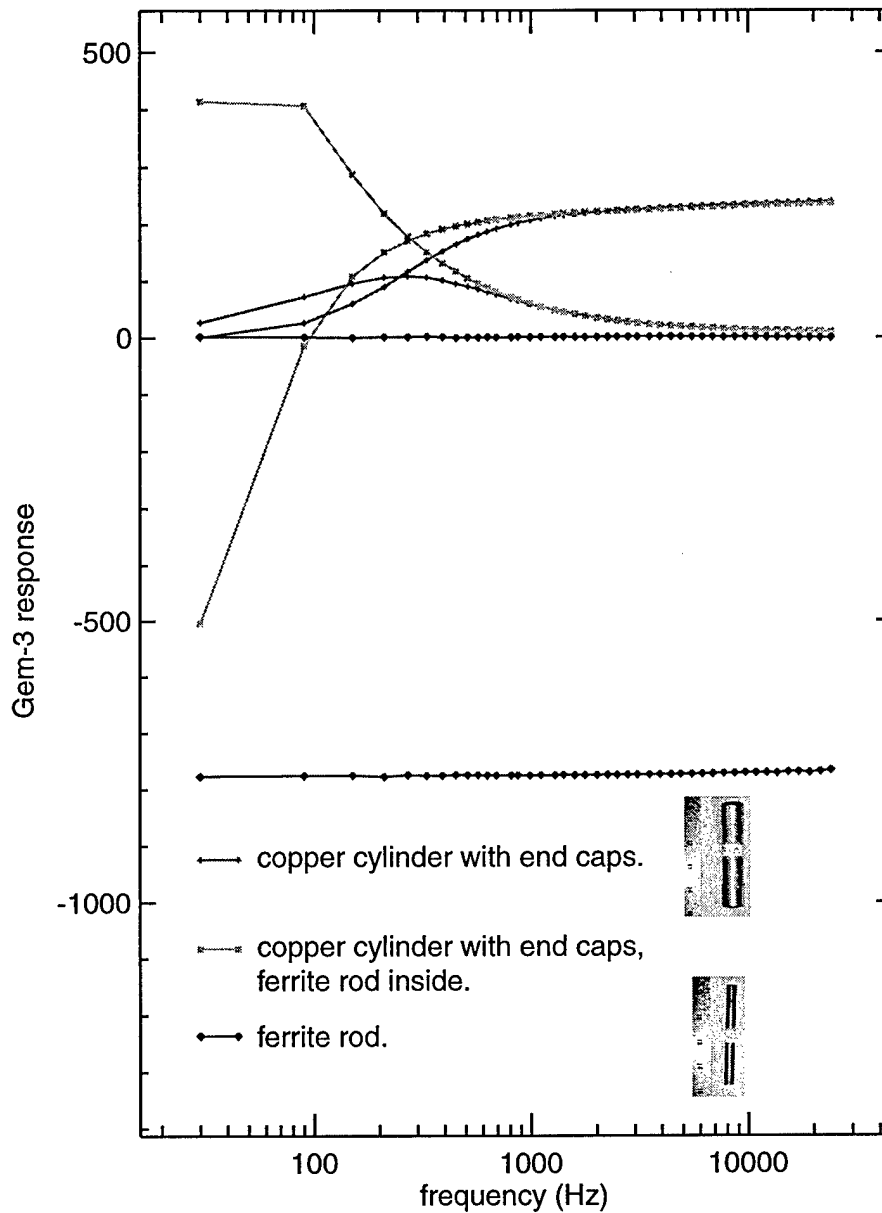
Figure 17. There is a complex interaction between the ferrite rod and surrounding copper pipe. At high frequencies, the pipe dominates, and at low frequencies, the ferrite dominates.

CONCLUSIONS

At this stage of the project, prospects are very good that broadband EMI will provide a useful basis for reliable UXO discrimination. We have solved problems collecting data with the GEM-3 sensor, so that our method now produces very accurate agreement with analytic models. We have collected a large amount of data on test objects and UXO and organized them in a database.

21

We have produced a simple 3-parameter baseline model for approximating EMI response from an arbitrary object, and confirmed that it produces reasonably good matches to a wide range of objects, and produces reasonable parameter values under most conditions.

We have shown that the information content available under field conditions is sufficient to observe strong differences in EMI response between UXO and non-UXO, and have made progress developing models to predict and describe these differences.

Analysis of our data indicates that subtle shape differences (e.g. cylinder with point vs. without) cannot be resolved reliably using EMI, but the presence of driving bands on projectile produce a strong and easily recognized signal. This appears to be a valuable feature to exploit in target discrimination.

We have published our results in technical presentations, conference papers, abstracts, and a database on the web.

REFERENCES

AETC 1999, Database of EMI results available for download from site: ftp.\\server.hgl.com. Login ID: "Anonymous", File: \pub\SERDP\GEM3_data.zip.

Bell, T, B. Barrow, and N. Khadr, 1998, "Shape Based Classification and Discrimination of Subsurface Objects Using Electromagnetic Induction". Presented at the International Geoscience and Remote Sensing Symposium (IGARSS '98). Seattle, Washington, July 6-10, 1998.

Grant, F. and G. West, 1965. Interpretation theory in applied geophysics: McGraw-Hill Book Co., New York, NY.

Moskowitz, R., E. Della Torre, and R. Chen, 1996. "Tabulation of Magnetometric Demagnetization Factors for Regular Polygonal Cylinders". Proceedings Letters, IEEE v.54 p.1211.

Ward, S. and G. Hohmann, 1987. "Electromagnetic Theory for Geophysical Applications", in Investigations in Geophysics no. 3, v1 : Electromagnetic Methods in Applied Geophysics. Society of Exploration Geophysics, Tulsa OK.

Appendix A

Paper to be presented at the Annual Symposium on the Application of Geophysics to Engineering and Environmental Problems (SAGEEP), 20-24, February, 2000, Arlington, Virginia.

ELECTROMAGNETIC INDUCTION RESPONSE OF SPHERICAL CONDUCTORS MEASURED WITH THE GEM-3 SENSOR, AND COMPARED TO ANALYTIC MODELS

J. Miller, B. Barrow, T. Bell, D. Keiswetter, and I. J. Won.

ELECTROMAGNETIC INDUCTION RESPONSE OF SPHERICAL CONDUCTORS MEASURED WITH THE GEM-3 SENSOR, AND COMPARED TO ANALYTIC MODELS

J. Miller, B. Barrow, T. Bell, *D. Keiswetter, and *I. J. Won

AETC Inc.   * Geophex, Ltd.
1225 Jefferson Davis Hwy Suite 800   605 Mercury St.
Arlington, VA 22202   Raleigh, NC 27603

ABSTRACT

Currently, most unexploded ordnance (UXO) remediation is carried out with magnetic and electromagnetic induction (EMI) sensors. While highly effective in detecting metallic objects such as UXO, present field techniques also result in many false targets from metallic scrap. To reduce the cost of digging non-UXO, discrimination techniques are required. One approach to UXO discrimination is to recognize features from broadband EMI data that reflect the shape of the target only, while filtering out other features which may relate to target depth, orientation, sensor-dependent signals, or combinations of these factors. A thorough calibration of the sensor against targets of known shape and material properties is required for proper interpretation of field data. Toward this goal, controlled measurements were made using the GEM-3 (FDEM) sensor on spherical conductors of various sizes at several distances. These data generally compare very well against the analytic solution for a sphere in a spatially uniform, time varying magnetic field, despite the fact that the GEM-3 sensor produces a primary field that is not spatially uniform.

BACKGROUND

In spite of the recent advances in UXO detection performance, false alarms due to clutter (signals incorrectly diagnosed as having been caused by UXO) remain a serious problem. With traditional survey methods, the Army Corps of Engineers finds that 85-95% of all detected targets are not UXO. Since the cost of identifying and disposing of UXO in the United States using current technologies is estimated to range up to $500 billion, increases in performance efficiency due to reduced false alarm rates can result in substantial cost savings.

Typical ordnance items have certain distinctive attributes that distinguish them from clutter. They have a characteristic shape (long and slender) and their composition is distinctive (typically comprising a steel body with a brass or aluminum fuze body and copper driving bands or an aluminum fin assembly). Our experience is that these attributes correspond to distinctive signatures in magnetic and electromagnetic induction sensor data. Current research activities are directed towards exploiting differences in shape between ordnance and clutter with commercially available sensors.
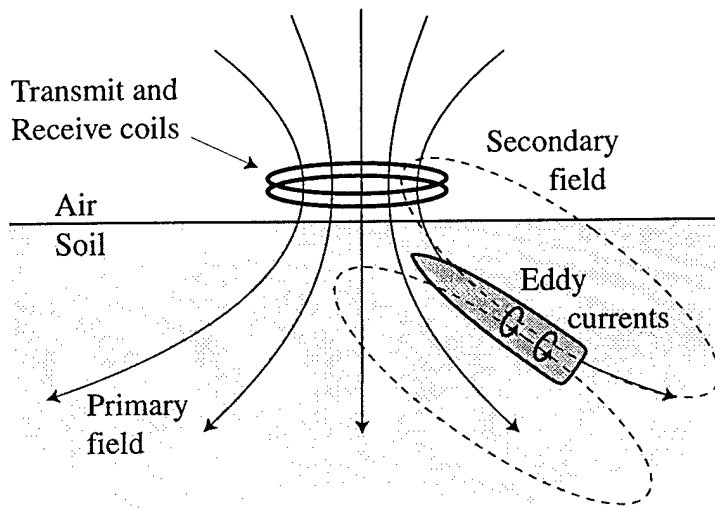
Figure 1. In response to a primary magnetic field, eddy currents develop within a
buried conducting target, producing a secondary magnetic field that can be measured
at the surface.

Electromagnetic induction (EMI) occurs when a time-varying primary magnetic field is
established over a buried conducting target. In response to the primary field, eddy currents
develop within the target, producing a secondary magnetic field that can then be measured at the
surface (figure 1). The secondary field depends on specifics related to the identity of the target
such as size, shape, composition, and orientation. For frequency domain electromagnetic
(FDEM) instruments, data from the sensor consists of the phase shift and amplitude of the
secondary field (figure 2).
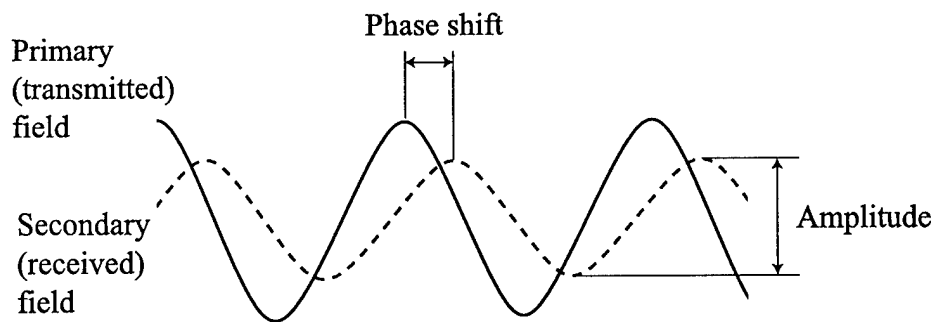
Figure 2. For frequency domain electromagnetic (FDEM) instruments, the phase shift
and amplitude of the secondary field contain information about the identity of the target.

The response for a given target depends both on the position and orientation of the sensor
relative to the target, and on the frequency of the primary field. Previously, an EMI response
model for compact conducting objects has been developed (Bell et. al. 1998) and successfully
used to invert EMI data (Barrow and Nelson, 1999) in order to estimate target specific
information. This model exploits the fact that the secondary field may be accurately described as
a dipole field in which total response is a linear combination of the actual response along each
principle axis of the target. Using this approach, spatially varying EMI data may be analyzed to
estimate the orientation and aspect ratio of the target.

Figure 3. Data for multiple sweeps on each object at different depths are overlayed in this graph, showing a strong relationship between the frequency dependent EMI response of a target and its shape and composition.
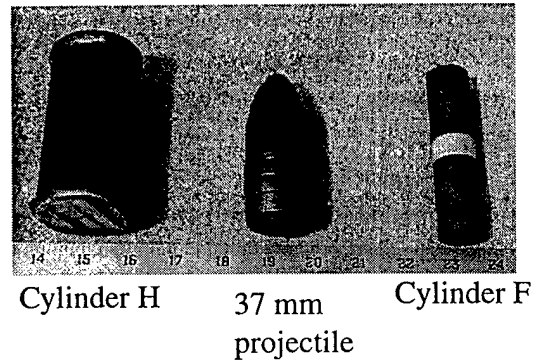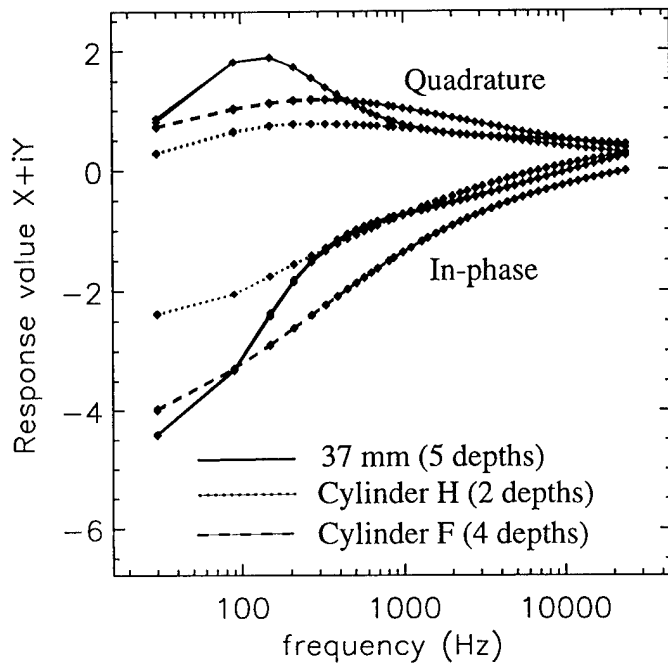
Current research is aimed at dramatically enhancing this approach by extracting additional shape information through analysis of frequency dependent EMI data. Experience has shown that there is a strong relationship between frequency dependent EMI response and the shape and composition of the target (figure 3). We are currently developing models that capture important aspects of this relationship, that are also simple enough to be used in an inversion scheme. As a first step toward model development, a careful calibration of the GEM-3 instrument was carried out using ferrite rod samples, and then data for metal spheres were compared against the analytical solution. Careful analysis of the agreement between these models and data provides an important reference point for development of more general models.

GEM-3 SENSOR

This project is ultimately aimed at developing a workable technique for discriminating UXO from clutter using existing commercial equipment. Therefore, any approach for data analysis must take into account the real-world performance characteristics of the commercial equipment in question. In this case, the GEM-3 sensor (figure 4) manufactured by Geophex Ltd. is being used. The GEM-3 employs a pair of concentric circular coils to generate the primary magnetic field, and current runs in opposite directions in these coils thereby setting up a zone of magnetic cavity at the center where the primary field strength approaches zero. A third receiving coil is placed within this magnetic cavity so that it senses only the weak secondary field resulting from eddy currents in the buried target. All coils are molded into a single circular disk in a fixed geometry and precisely known dimensions.
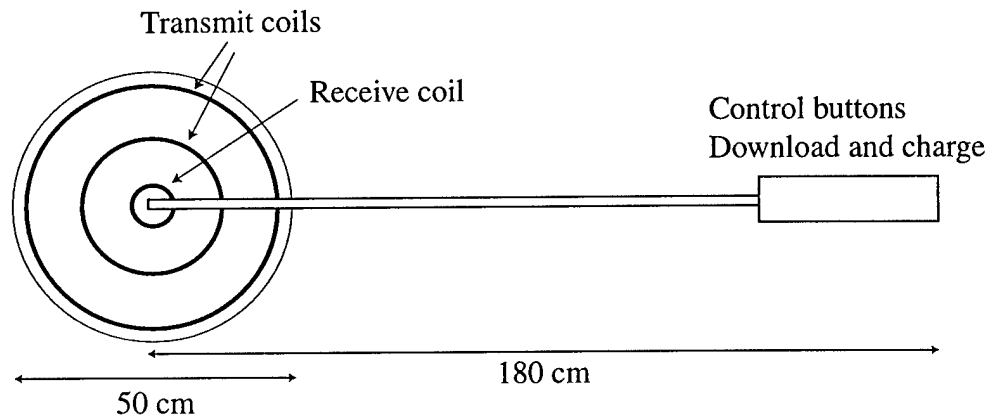
Figure 4. The GEM-3 instrument.

More than 60,000 EMI measurements were collected on a variety of objects including rods, spheres, and UXO using the GEM-3. The instrument was suspended in a wooden frame, leveled, and all dimensions were carefully measured (figure 5). The complete data set can be downloaded as an ACCESS database on the SERDP ftp site: ftp:\\server.hgl.com
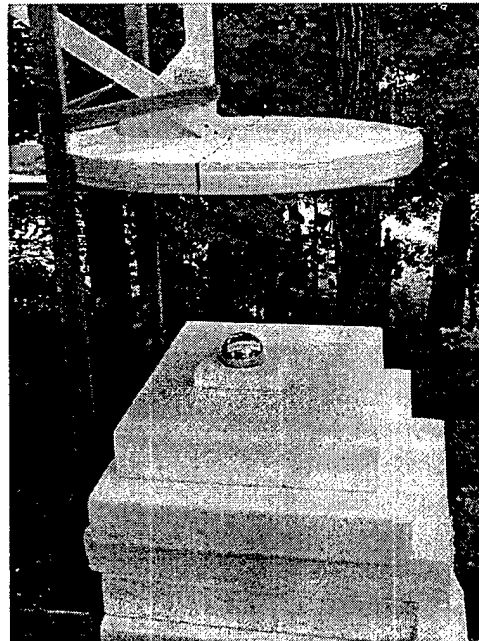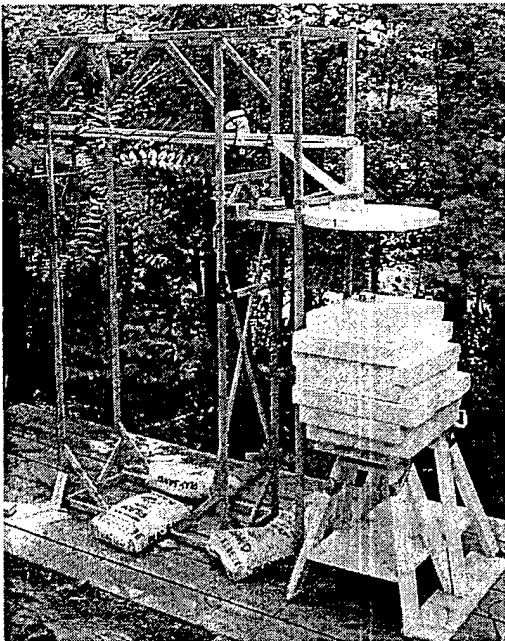
Figure 5. EMI data was collected on a variety of objects including metal spheres using the GEM-3 supported in a wooden frame.

ANALYTICAL MODEL FOR SPHERES

As a first step toward developing mathematical expressions to describe aspects of EMI data collected with the GEM-3, we need to analyze the agreement between GEM-3 data and the analytical solution for metal spheres. The EMI response of a permeable conducting sphere in a spatially uniform, time-varying primary field is a magnetic dipole with moment m given by Grant and West, 1965;

$$m = -2\pi a^3 H_0 e^{i\omega t} (X + iY)$$

where

a = radius of sphere.

H_0 = amplitude of the primary field.

ω = frequency.

t = time.

The term $(X+iY)$ is the response function for a sphere, given by:

$$(X + iY) = \left\{ \frac{(1 + k^2 a^2 + 2\mu)\ \sinh(ka) - (2\mu + 1)\ ka\ \cosh(ka)}{(1 + k^2 a^2 - \mu)\ \sinh(ka) + (\mu - 1)\ ka\ \cosh(ka)} \right\}$$

where

$k^2 = i\sigma\mu\omega$

σ = conductivity.

μ = relative permeability.
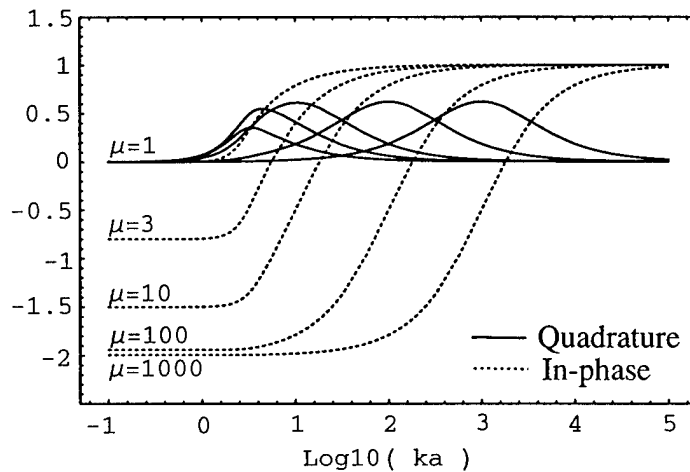
Figure 6. Analytical solution for the response of a permeable conducting sphere in a spatially uniform time-varying primary field. The parameter μ is relative permeability.

SPHERE MODEL FIT TO GEM-3 DATA

The analytical sphere model was fit to EMI data from several metal spheres ranging in diameter from 5/8 inch to 5 inches. Metals included chrome steel, stainless steel, aluminum, bronze, and brass. In every case very good agreement between GEM-3 data and the model was achieved. Results for the 3-inch diameter chrome steel ball are shown here.

These data come from measurements on the 3 inch diameter chrome steel sphere at 6 different ranges from 20 cm to 66 cm, measured to the center of the sphere. Fitted parameters are relative permeability, conductivity, and an amplitude coefficient applied to the data to account for drop in signal strength with range. The fit is within about 1 percent at frequencies below 1000 Hz, and within about 0.2 percent above 1000 Hz. The fit improves with higher frequency because greater power is transmitted and the signal to noise ratio improves.
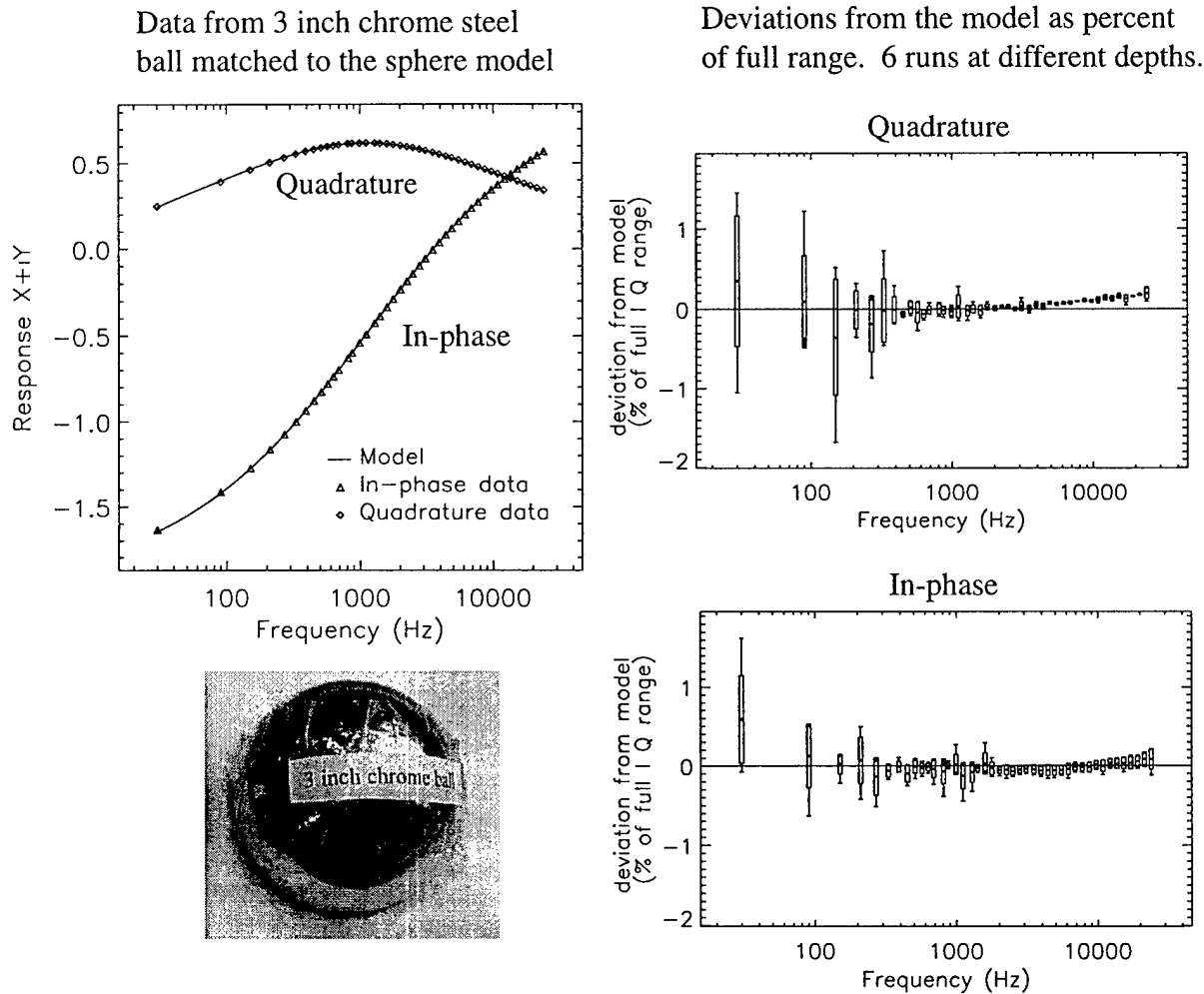
Figure 7. Data collected with the GEM-3 fits the analytical sphere model about one percent or better.

Generally, data from the GEM-3 compares very well against the analytical solution for a sphere in a spatially uniform, time varying magnetic field, despite the fact that the GEM-3 produces a primary field that is not spatially uniform.

<div align="center">Fitted Parameters for 3-inch Chrome Steel Ball</div>

Fitted model parameters for the 3-inch chrome ball were compared against published values. Values for the exact metal in our sample were not found in the literature, so similar metals were used for comparison. The fitted value for relative permeability compares with values extrapolated from literature sources for similar metals (figure 8).
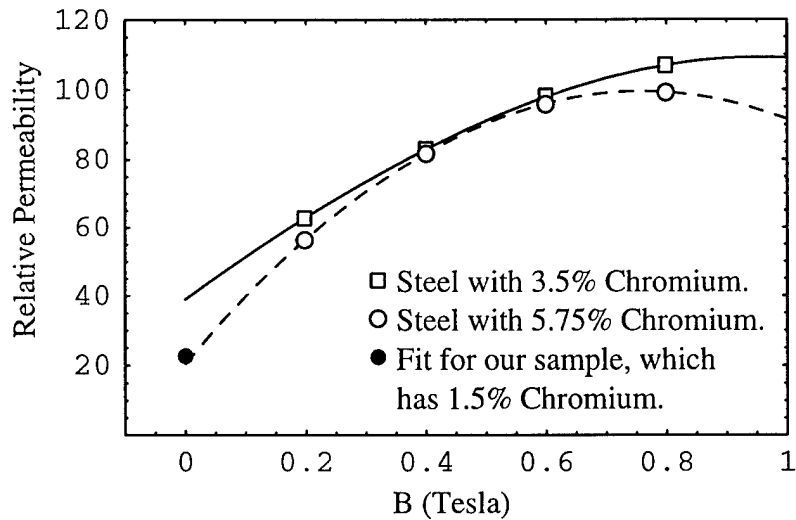
Figure 8. Fitted relative permeability for our sample compares with values extrapolated from literature. Source: Smithsonian Physical Tables, Forsythe, 1969.

The fitted value for conductivity also compares with values for similar metals (table 1).

	Conductivity (mho/m)
Estimate for our sample	1.82 E 6
Plain carbon steel type AISE-SAE 1020	1.0 E 7
Stainless steel type 304	1.39 E 6

Table 1. The estimated conductivity for the 3-inch steel ball compares well with published values for similar metals. Source: CRC Handbook of Chemistry and Physics p. D-171 (Weast, 1976).

The fitted value for conductivity also compares with values for similar metals (table 1).

CONCLUSIONS

These results prove that the GEM-3 instrument is capable of producing data that accurately matches known analytical solutions, and lead to parameter estimates which compare well with known values. Importantly, this provides a validated starting point for future development of more general models to describe important aspects of EMI response of arbitrary objects.

The sphere model given above is for the case of a spatially uniform primary field. An analytic solution is also available for the case of a dipole primary field, which may be a better approximation of the primary field generated by the GEM-3. However that solution is more complicated, consisting of a summation of terms representing dipole, quadrupole, and octopole, etc., components. The fact that close agreement was found between the uniform-field model and data from the GEM-3 shows that the higher order terms, i.e., quadrupole, octopole, etc. may be safely ignored for the dimensions and geometries used in this study. Measurements in this data set were collected with the sphere generally farther than one diameter length away from the sensor, and since higher order terms fall off more rapidly with distance, it follows that the dipole term should dominate as distance increases.

REFERENCES

Bell, T., B. Barrow, and N. Khadr, 1998, "Shape-Based Classification and Discrimination of Subsurface Objects Using Electromagnetic Induction", International Geoscience and Remote Sensing Symposium (IGARSS '98), Seattle, Washington, July 6-10, 1998.

Barrow, B. and H. Nelson, 1999, "Model-Based Characterization of EM Induction Signatures for UXO/Clutter Discrimination Using the MTADS Platform", UXO Forum 1999, Atlanta, Georgia, May 25-27, 1999.

Grant, F. and G. West, 1965, Interpretation theory in applied geophysics: McGraw-Hill Book Co., New York, NY.

Forsythe, W. E. editor , 1969, Smithsonian Physical Tables, 9th revised edition: Smithsonian Institution Press, Washington D.C.

Weast, R. C. editor, 1976, Handbook of Chemistry and Physics, 56th edition. CRC Press, Cleveland OH.

Appendix B

Paper to be presented at the Annual Symposium on the Application of Geophysics to Engineering and Environmental Problems (SAGEEP), 20-24, February, 2000, Arlington, Virginia.

ELECTROMAGNETIC INDUCTION SPECTROSCOPY FOR LANDMINE IDENTIFICATION

I. J. Won and Dean Keiswetter

ELECTROMAGNETIC INDUCTION SPECTROSCOPY
FOR LANDMINE IDENTIFICATION

I.J. Won and Dean Keiswetter
Geophex, Ltd.
605 Mercury Street
Raleigh, NC 27603

Thomas H. Bell, Jonathan Miller, and Bruce Barrow
AETC, Inc.
1225 Jefferson Davis Highway
Arlington, Virginia 22202

ABSTRACT

An estimated 110 million landmines, mostly antipersonnel mines laid in over 60 countries, kill or maim over 26,000 people a year. One of the dilemmas for removing landmines is the amount of false alarms in a typical minefield. Broadband electromagnetic induction spectroscopy (EMIS), however, is a promising technology that can both detect and identify buried objects as landmines. By reducing the number of false alarms, this approach significantly reduces costs associated with landmine removal. Combining the EMIS technology and a broadband EMI sensor, the scientific phenomenology that has potential applications for identifying landmines, unexploded ordnance, and hidden weapons at security checkpoints can now be explored.

INTRODUCTION

According to United Nations statistics, an estimated 110 million landmines, mostly antipersonnel (AP) mines laid in over 60 countries, kill or maim over 26,000 people a year. While an international treaty banning the AP mines, thus removing the source, is getting popular support, many organizations, including the U.S. government, have invested in the "humanitarian de-mining" effort to remove existing landmines from the earth.

Clearing a landmine requires two-steps: detection and removal. The most common tools used to find landmines are metal detectors and, less commonly, magnetometers. These sensors are relatively simple to use, light, and affordable, a factor particularly important in developing countries where these mines are buried. Other potential sensors, e.g., ground-penetrating radar, are still in the research or prototype stages, and their ultimate utility for landmine detection is not certain at this time.

Landmines are cheap to make, commonly costing less than a few dollars a piece. Yet, it costs several hundred dollars to remove each landmine. Some so-called "plastic mines" contain only a small amount of metal and, thus, often are hard to find with metal detectors. The overriding reason for the high removal cost, however, is not the difficulty in detecting landmines but the amount of clutter in typical minefields. The clutter may be natural (e.g., magnetic rocks) or manmade objects (e.g., nails, pull-tabs, and metal cans) that trigger the sensor in a way similar to a real mine. When its identity is unknown, each clutter item must be treated as a landmine during the removal, which is the most painstaking, time-consuming, and costly phase of the job.

Often as many as 95% of suspected anomalies are non-ordnance items (1). At this clutter rate, the cost of landmine removal becomes so high that no society can afford it. The most desirable solution is to come up with smart sensors that can reduce the clutter by identifying it as such and, thus, eliminate the need of excavation except for real mines. We present in this article such an approach, one that uses broadband electromagnetic induction spectrum.

ELECTROMAGNETIC INDUCTION SPECTROSCOPY

An object, made partly or wholly of metals, has a distinct combination of electrical conductivity, magnetic permeability, and geometrical shape and size. When the object is exposed to a low-frequency electromagnetic field, it produces a secondary magnetic field. By measuring the broadband spectrum of the secondary field, we obtain a distinct spectral signature that may uniquely identify the object. Based on the response spectrum, we can "fingerprint" the object. This is the basic concept of *Electromagnetic Induction Spectroscopy (EMIS)* (2).

When an electrically conductive and/or magnetically permeable object is placed in a time-varying electromagnetic field, a system of induced current flows through the object. By observing the small secondary magnetic field emanating from the induced current, we attempt to detect the object; this is the foundation of the well-known electromagnetic induction (EMI) method. Although EMI physics is completely described by Maxwell's four equations, analytical solutions beyond the simplest geometry are rare due to mathematical complexity.

The EMI principle is the basis of common metal detectors used for airport security checks as well as for treasure hunting on the beach. They are popular, inexpensive, and common. They cannot, however, distinguish one metallic object from another, so that the number of false targets generally far exceeds that of real targets. In other words, they detect metal objects indiscriminately and, thus, produce much wasted effort in excavating false targets.

EMIS technology explores the frequency dependence of the EMI response. By measuring an object's EMI response in a broad frequency band, we attempt to detect and characterize the object's geometry and material composition. Electromagnetic theory shows that an object must exhibit different responses at different frequencies. This fact has not been exploited because there have been no practical broadband EMI instruments to study the phenomenon. Most commercial EMI sensors (including common metal detectors) operate at single frequency or, rarely, at a few discrete frequencies. However, with the recent development of broadband EMI sensors, it is now possible to exploit broadband EMI spectra in order to detect and identify the targets.

BROADBAND EMIS SENSOR

To explore EMIS-based landmine identification, we have employed the GEM-3 (Figure 1), a monostatic, broadband, electromagnetic sensor designed for subsurface geophysical investigation. Because the GEM-3 sensor details have been discussed in detail – including an analytic description of the transmitted and received fields (3, 8) - only a summary of the sensors salient features are presented here.

The GEM-3 operates in a bandwidth from 30 Hz to 24 kHz. The sensing head consists of a pair of concentric, circular coils that transmit a continuous, broadband, digitally controlled, electromagnetic waveform. The two transmitter coils connected in an opposing polarity, with precise dimensions and placement, create a zone of magnetic cavity (viz., an area with a

vanishing primary magnetic flux) at the center of the two coils. A magnetic cavity is defined as a region where a directional sensor, placed in a specified orientation, produces zero signal induced from the magnetic field. It has been shown (3, 8) that a magnetic cavity can be created at the center of two concentric, circular, current loops that are electrically connected in series into one circuit. The GEM-3's receiving coil is placed within this magnetic cavity so that it senses only the weak, secondary field returned from the earth and buried targets (Figure 2)(3).

The GEM-3 is a transmitter-bucked sensor, and its concentric geometry is called a "monostatic" configuration because all coils are co-located (3). The coils are molded into a single, light, circular disk in a fixed geometry, rendering a very portable package. The disk, along with a handle boom, is made of a Kevlar-skinned foam board. Attached to the other end of the boom is a removable electronic console (Figure 1). The entire unit weighs about 4 kg.
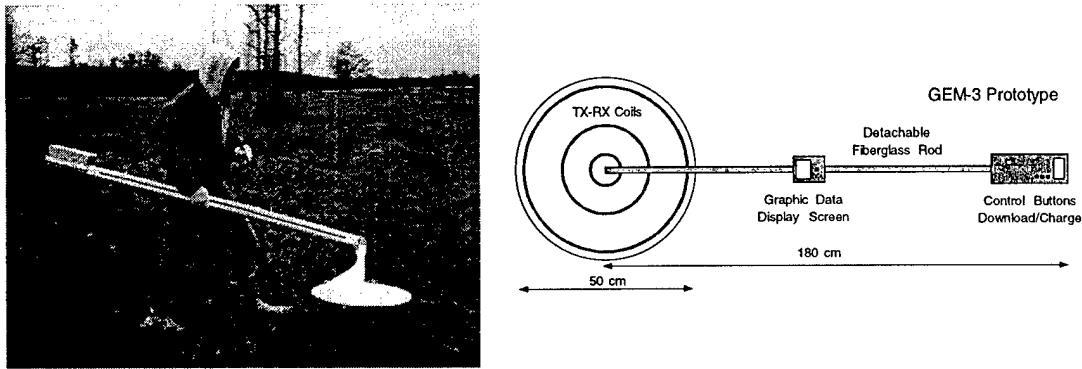
Figure 1. Left – Photograph of the GEM-3 monostatic broadband EMI sensor. Right - Schematic diagram showing its internal construction.
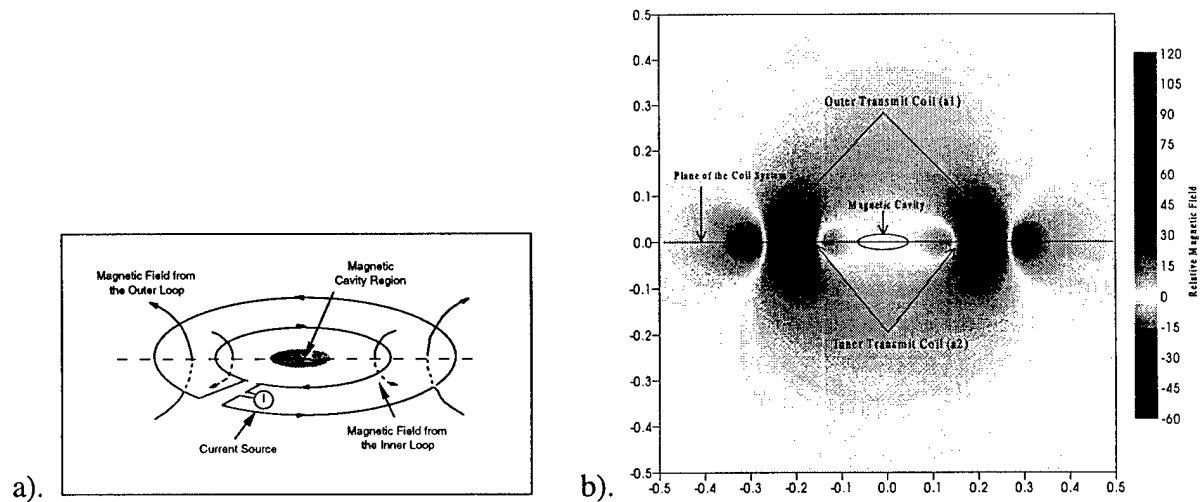
Figure 2. (a) Conceptual representation of creating a central magnetic cavity region using two concentric, circular loops that are electrically connected in an opposing polarity. (b) Vertical component of the magnetic field that results from two concentric coils. Notice that the effect of the opposing coil is negligible in the far field. The amplitude scale is normalized to $\frac{\mu_0 I}{2}$.

THEORETICAL AND EXPERIMENTAL EMIS DATA

To establish the validity of the GEM-3 frequency response, we measured the spectral response of many metal spheres and ancillary calibration targets (i.e., Q-coils). Spheres are one of the few geometrical shapes for which rigorous analytic solutions are available (5). An EMI response is a complex quantity; its real part is called the "inphase" component while the imaginary part is called the "quadrature" component.

Figure 3 shows a comparison between the computed (solid lines) and observed (various symbols) EMIS spectra, consisting of the inphase and quadrature components, for a three-inch chrome sphere measured in air. The analytical model to calculate the spheres response was (5):

$$X + iY = \left\{ \frac{[\mu_0(1+k^2a^2)+2\mu\mu_0]\sinh(ka)-(2\mu\mu_0+\mu_0)ka\cosh(ka)}{[\mu_0(1+k^2a^2)-\mu\mu_0]\sinh(ka)+(\mu\mu_0-\mu_0)ka\cosh(ka)} \right\},$$

where

μ_0 = Permeability of free space = $4\pi \times 10^{-7}$ (N/A^2)

μ = Relative permeability of the object = μ_{object} / μ_0

$k = i\sigma\mu\omega$ (1/m)

σ = Conductivity of the object (Mho/m)

ω = Frequency (Rad/s)

a = Radius of the sphere or cylinder (m)

J_n = Bessel function of order n

$\alpha = a(1-i)\sqrt{\sigma\mu\omega/2}$

$X + iY$ = Response value

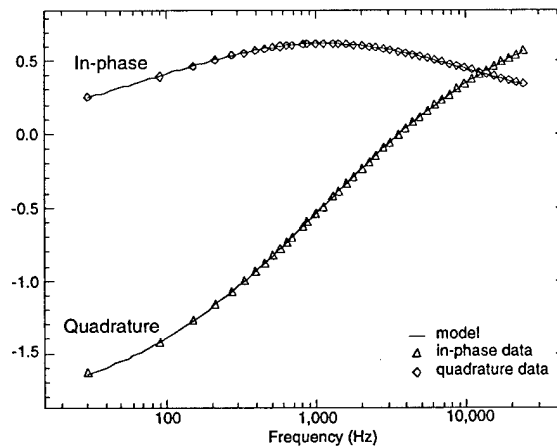Figure 3. GEM-3 data from a three-inch diameter chrome steel sphere compared to the sphere model (measured in air at a height of 37.3 cm).

Although the conductivity and permeability values for the calibration chrome sphere are not available, we can estimate these explanatory variables (by minimizing the residual during the sphere fitting algorithm), and then compare the model parameters with published values. A

comparison of the model parameters (conductivity and permeability) with published values for similar metals are shown in Figure 4.

Conductivity:

Estimate for three-inch Sphere	1.82E6 mho/m
Plain carbon steel (AISI-SAE 1020)	1.E7 mho/m
Stainless steel type 304	1.39E6 mho/m

Permeability
Curve fits to published mu values
for two similar chrome steels.
(From Smithsonian Physical Tables)
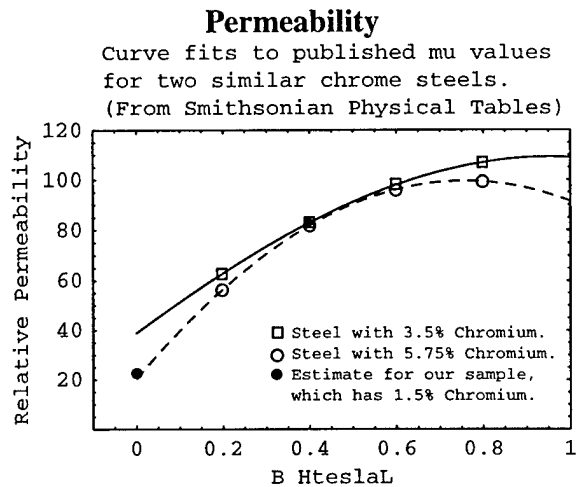
Figure 4. Comparison between model fits of conductivity and permeability to published values for similar metals.

SPECTRAL RESPONSE OF LANDMINES

Figure 5 shows the EMIS spectra (measured in air) for seven common landmines, along with their photographs. Shown on the right is the commentary on the construction and detectability of each mine (7). Two mines in Figure 5, M-14 and PMA-3, are common plastic mines that have very small metallic parts in their pressure activation mechanisms. As expected, the two plastic mines show the smallest amplitudes, less than 0.1 ppm. Yet, Figure 5 indicates that the metal parts are not only clearly detectable by the GEM-3 but also render specific EMIS spectra.

The unit used to show the sphere response along the vertical axes in Figure 5 is part-per-million (or ppm) defined as the ratio

$$ppm\ response\ unit = \frac{secondary\ magnetic\ field\ at\ receiver\ coil}{primary\ magnetic\ field\ at\ receiver\ coil} \times 10^6.$$

We note from Figure 5 that the EMIS spectrum of each landmine is unique and clearly distinguishable from other landmines. At the same time, these spectra may be considered bland in the sense that they lack the sharp peaks in, say, a gamma-ray radiation spectrum. To make up its blandness, the EMIS spectra contain (1) inphase and quadrature components, and (2) positive and negative polarities; thus, EMIS spectrum contains as many distinguishing attributes as do spectra with sharp peaks.

In addition to their general spectral shapes, some obvious EMIS attributes include (1) response amplitude, (2) peak frequency in quadrature, (3) zero-crossing frequency in inphase, (4)

phase angle, i.e., the ratio between the two components, and (5) negative inphase at low frequencies for ferrous metals. We note from Figure 5 that two mines, TS-50 and PMA-3, contain mostly nonferrous metals (because of only positive inphase), while others are made of mostly ferrous metals in various proportions. Also note that for three mines, TS-50, VS-50, and PMN-6, the spectra lack peaks in the quadrature, indicating that the GEM-3 bandwidth may be further broadened.

In order to show the method's target identification (or clutter elimination) potential, we compare in Figure 6 the EMIS spectra of an M-14 landmine and several common clutter items. Again, we note that each EMIS spectrum is unique, implying that we should be able to identify an individual object based on the EMIS response.

DISCUSSION

As shown in Figures 3 and 4, the GEM-3 sensor is capable of accurately and reliably measuring the broadband EMI spectral response of small targets – including landmines. All data presented herein were acquired in air and therefore neglected the response of soil materials. Because certain soil types, such as magnetic rocks of laterite soils, may complicate the analysis of EMIS data for low-metal content mines, we chose to conduct controlled experiments in air to demonstrate the techniques potential. The effects of competing factors, including soil type and proximity to ancillary clutter, are an area of active research. These spectral data indicate that the landmines included in this analysis possess distinct spectral signatures when the competing factors are ignored.

As described above, a general approach for identifying specific landmines, as well as for discriminating between landmines and clutter, is to compare the sensor response to a library of signatures. This often includes a preprocessing step that fits the data to a dipole model, from which estimates of the target orientation and depth can be derived. Once this is done, the target can be effectively rotated into a principal axis coordinate system and the spectral response in this system can be compared to the library responses. Another way to state this is that the eigenvalues of the magnetic polarizability tensor that models the target are derived from the data. These eigenvalues are orientation invariant and can be used as intrinsic target signatures (9). In this paper, however, we examined the inphase and quadrature components for a fixed orientation. Future work will combine both the orientation and range invariant aspects of the problem into a single procedure.

FUTURE DEPLOYMENT

In a simple scenario, consider an EMIS-based mine detector that has in its memory the spectral signatures of all known landmines. The detection phase can be accomplished using a few discrete frequencies that are chosen to be optimal for a given geologic and cultural environment. Once a target is suspected, we start the identification phase that involves recording the target's spectral response. The measured spectrum may be scanned through the signature memory in order to identify a particular landmine or, if no match is found, to reject the target as a clutter item. A given minefield would likely contain only one or, at most, a few types of mines, which would considerably simplify the identification process.

Experiments have shown that the EMIS spectrum of a spherical target (or one that, owing to its aspect ratio, can be approximated as such) in the far field is independent of the sensor view

angle. Under this condition, the dependence on distance is quite predictable: the spectral amplitudes change, but their shapes do not. Commonly, landmines are cylindrically symmetric and laid flat for vertical pressure activation. Since the GEM-3 also has a cylindrical symmetry, the mutual view is fixed when the sensor is directly above the mine.

In general, however, the EMIS spectrum is dependent on the target's view from the sensor, just as a person may look different from different angles. This view-dependency of the EMIS spectrum is a serious drawback since it requires storing an infinite number of views of a target in order to match an observed EMIS spectrum of a hidden target with an unknown view.

Theoretically speaking, however, if we have at least three orthogonal views of an object, we then have a "complete" view; thus, the object can be identified. For instance, if an object's EMIS spectra are recorded from three principal views (e.g., one top view and two side views), it can be identified from any angle through a coordinate rotation. For a buried object, however, we do not know how much to rotate to match the stored views. This is one of the subjects that need a concentrated effort to advance EMIS technology to its full potential.

Theoretical and experimental work to date suggests that these potentials are well-worth pursuing. For the past year, we have conducted field tests of EMIS-based sensors under a variety of conditions with extremely promising results. We hope that increased knowledge of EMIS will lead to development of second- and third-generation EMIS-based sensors that can address current and future landmine detection challenges throughout the world.

REFERENCES

1. Report to the U.S. Congress, *Unexploded Ordnance Clearance: A Coordinated Approach to Requirements and Technology Development,* Office of the Under Secretary of Defense, 25 March 1998.
2. I.J. Won, D. Keiswetter, and E. Novikova, 1998, *J. Environ. Eng. Geophysics,* 3, 27 (1998).
3. I.J. Won, D. Keiswetter, D. Hanson, E. Novikova, and T. Hall, *J. Environ. Eng. Geophysics,* 2, 53 (1997).
4. I.J. Won, D. Keiswetter, G. Fields, and L. Sutton, 1996, *J. Environ. Eng. Geophysics,* 1, 129 (1996).
5. F.S. Grant and G.F. West, *Interpretation Theory in Applied Geophysics,* (McGraw-Hill Book Co., New York, 1965); G.S. Lodha and G.F. West, *Geophysics,* 41, 1157 (1976); J. R. Wait, *Geophysics,* 16, 666 (1951); J. R. Wait, *Canadian J. Physics,* 31, 670 (1953); J. R. Wait, 1959, *J. Res. National Bureau of Standards,* 64B, 15 (1959); J. R. Wait, *Geophysics,* 25, 619 (1960); J. R. Wait, *Geophysics,* 34, 753 (1969).
6. *Handbook of Chemistry and Physics,* Weast, R. Ed. (Chemical Rubber Co., Cleveland, Ohio, 1972).
7. Mine Recognition and Warfare Handbook (U.S. Army Engineer Center, Fort Monroe, VA, 1990).
8. D. Keiswetter, E. Novikova, I.J. Won, T. Hall, and D. Hanson, 1997, *SPIE,* Vol. 3079.
9. D. Keiswetter, I.J. Won, B. Barrow, and T. Bell, 1999, *SAGEEP* Proceedings, p. 743-751.

Appendix C

Abstract for a poster presented at the SERDP Partners in Environmental Technology Symposium, December 2, 1999, Arlington, Virginia.

TARGET-SPECIFIC INFORMATION CONTENT IN BROADBAND EMI DATA

J. Miller, D. Keiswetter, T. Bell, B. Barrow, and I. J. Won.

Title: TARGET-SPECIFIC INFORMATION CONTENT IN
                     BROADBAND EMI DATA
Author: Jonathan Miller
Organization: AETC Incorporated
Street Address: 1225 Jefferson Davis Highway, Suite 800
City State Zip: Arlington, VA 22202
Phone: (703) 413-0500
email: jtmiller@va.aetc.com
co-authors: Dean Keiswetter, Thomas Bell, Bruce Barrow, I. J. Won
body:

Electromagnetic induction (EMI) occurs when a time-varying primary magnetic field is established over a buried conducting target. In response to the primary field, eddy currents develop within the target, producing a secondary magnetic field that can then be measured at the surface. The secondary field depends in part on specifics related to the identity of the target such as size, shape, composition, and orientation, but also in part on competing effects such as conducting soils, depth effects due to non-uniformity of the primary field, and inhomogeneous material properties within the target. These competing effects act to obscure some of the target-specific information, and it is therefore crucial to understand how much target-specific information is available in the raw data before any target identification scheme can go forward.

We present here results of controlled measurements made with the GEM-3 sensor to address this question. Several potential competing effects are evaluated and generally found to cause 1 percent or less deviation in the baseline signal for the objects tested. Generally, much larger differences were measured as a result of switching targets. In particular, the difference between a 37-mm projectile and a cylinder of roughly the same size was about an order of magnitude larger than any competing effect. The frequency-dependent structure of the difference was also reproducible and consistent over a range of depths. Therefore, we have established that this instrument is capable of delivering broadband EMI data with ample target-specific information content for the purpose of target classification and identification.

Appendix D

DISCRIMINATING CAPABILITIES OF MULTIFREQUENCY EMI DATA

D. Keiswetter, I. J. Won, J. Miller, T. Bell.

1. Submit to: AM101, NGUYEN

2. Discriminating Capabilities of Multifrequency EMI Data

3.   Dean Keiswetter, Geophex, 605 Mercury Street, Raleigh NC, ph: 919-839-8515, fax: 919-839-8528, keiswetter@geophex.com
I.J. Won, Geophex, 605 Mercury Street, Raleigh NC, ph: 919-839-8515, fax: 919-839-8528, ijwon@geophex.com
Jonathan Miller, AETC Incorporated, 1225 Jefferson Davis Highway, Suite 800, Arlington, Virginia 22202, ph: 703-413-0500, fax: 703-413-0512, jmiller@va.aetc.com
Tom Bell, AETC Incorporated, 1225 Jefferson Davis Highway, Suite 800, Arlington, Virginia 22202, ph: 703-413-0500, fax: 703-413-0512, tbell@va.aetc.com

4. Presentation: Oral

5. Abstract Text:

Although commercially available geophysical sensors are capable of detecting UXO at nominal burial depths, they cannot reliably discriminate between UXO and clutter. As a result, an estimated 75% of remediation funds are spent on nonproductive excavations. During the past few years, we have been studying the merits of using multifrequency EMI data for discriminating between UXO and non-UXO targets and believe the method has tremendous potential. The EMI spectral response of an object is a function of its electrical conductivity, magnetic permeability, shape, size, and orientation relative the primary exciting field. By measuring a target's spectral response, we obtain its characteristic frequency-dependent signature. Based on the response spectrum, we "fingerprint" the object and compare its response to known UXO signatures. To explore this phenomenon, we have developed a unique, frequency-domain EMI sensor named the GEM-3, which operates over a bandwidth of 30 Hz to 24 kHz. Empirical data acquired using the GEM-3 for a wide assortment of UXO and non-UXO suggests strongly that the EMI anomaly measured in a broad band offers an ability to both detect and identify a target. We present results of controlled measurements made with the GEM-3 sensor to address the question of competing effects such as sensor stability, depth and shape effects, and inhomogeneous material properties. The frequency-dependent signatures are reproducible and consistent over a range of depths. Therefore, we have established that the GEM-3 is capable of delivering broadband EMI data with ample target-specific information for the purpose of target classification and identification.

6. Keywords: Electromagnetic Induction Spectroscopy, UXO, Discrimination, GEM-3, Electromagnetic Induction

7. Biography:

Dean Keiswetter received Ph.D. and M.S. degrees in geophysics from the University of Kansas in 1995 and 1992 respectively, and a B.S. degree in geology at Fort Hays State

University in 1989. Currently, Dean is the Program Manager of the Geophysics Division and Deputy Manager of the Research and Development Division at Geophex, Ltd. Geophex is an environmental and engineering firm that specializes in the design and development of electromagnetic instruments. His research activities include the advancement of electromagnetic sensors and the applications of EM, magnetic and seismic methods to environmental and geotechnical problems. He is a member of SEG, NSG, ASEG, and EEGS.

Appendix E

ELECTROMAGNETIC INDUCTION SPECTROSCOPY FOR DETECTING AND IDENTIFYING BURIED OBJECTS

D. Keiswetter, I. J. Won, J. Miller, T. Bell.

Electromagnetic Induction Spectroscopy for Detecting and Identifying Buried Objects

Dean Keiswetter, I.J. Won, Jonathan Miller*, and Tom Bell*
Geophex, Ltd.
605 Mercury Street
Raleigh, North Carolina 27603
Phone: (919) 839-8515
Fax: (919) 839-8528
Email: keiswetter@geophex.com

*AETC Incorporated
1225 Jefferson Davis Highway, Suite 800
Arlington, Virginia 22202

An object, made partly or wholly of metals, has a distinct combination of electrical conductivity, magnetic permeability, and geometrical shape and size. When the object is exposed to a low-frequency electromagnetic field, it produces a secondary magnetic field. By measuring the broadband spectrum of the secondary field, we obtain a distinct spectral signature that may uniquely identify the object. Based on the response spectrum, we attempt to "fingerprint" the object. This is the basic concept of Electromagnetic Induction Spectroscopy (EMIS). From numerous surveys that we have conducted using our multifrequency electromagnetic sensors (GEM-2 and GEM-3 developed by Geophex), we have accumulated significant evidence that a metallic object undergoes continuous changes in response as the transmitter frequency changes. These observations made over many UXO targets suggest strongly that the EMI anomaly measured in a broad band offers an ability to both detect and identify a target. We present results of controlled measurements made with the GEM-3 sensor to address the question of competing effects (viz., conducting soils, depth effects, and inhomogeneous material properties within the target). Several potential competing effects are evaluated and generally found to cause 1 percent or less deviation in the baseline signal for the objects tested. The frequency-dependent structure of the difference was also reproducible and consistent over a range of depths. Therefore, we have established that the GEM-3 is capable of delivering broadband EMI data with ample target-specific information content for the purpose of target classification and identification.

Appendix F

Abstract submitted to the International Geoscience and Remote Sensing Symposium (IGARSS),
July 24-28, 2000, Honolulu, Hawaii

DISCRIMINATING CAPABILITIES OF MULTIFREQUENCY EMI DATA

D. Keiswetter, I. J. Won, J. Miller, T. Bell

Discriminating Capabilities of Multifrequency EMI Data

Dean Keiswetter, I.J. Won, Jonathan Miller*, and Tom Bell*
Geophex, Ltd.
605 Mercury Street
Raleigh, North Carolina 27603
Phone: (919) 839-8515
Fax: (919) 839-8528
Email: keiswetter@geophex.com

*AETC Incorporated
1225 Jefferson Davis Highway, Suite 800
Arlington, Virginia 22202

Commercially available geophysical sensors, primarily magnetometers, metal detectors, and time-domain EM, are capable of detecting UXO at nominal burial depths. The significantly large number of false alarms that these sensors produce, however, plagues UXO-cleanup programs. The ability to distinguish if a particular target is UXO or not, based on its measured signature, would dramatically reduce remediation costs. During the past few years, we have been studying the merits of using multifrequency EMI data for discriminating between UXO and non-UXO targets and believe the technique has tremendous potential. The EMI spectral response of an object is a function of its electrical conductivity, magnetic permeability, shape, size, and orientation relative the primary exciting field. By measuring a target's spectral response, we can obtain its characteristic frequency-dependent signature. Based on the response spectrum, we attempt to "fingerprint" the object and compare its response to known UXO signatures. This is the basic concept of Electromagnetic Induction Spectroscopy (EMIS). To explore this phenomenon, we have developed a unique, frequency-domain EMI sensor named the GEM-3, which operates over a bandwidth of 30 Hz to 24 kHz. Empirical data acquired using the GEM-3 for a wide assortment of UXO and non-UXO suggests strongly that the EMI anomaly measured in a broad band offers an ability to both detect and identify a target. We present results of controlled measurements made with the GEM-3 sensor to address the question of competing effects such as sensor stability, depth and shape effects, and inhomogeneous material properties. Several potential competing effects are evaluated and generally found to cause one percent or less deviation in the baseline signal for the objects tested. The frequency-dependent structure of the difference is reproducible and consistent over a range of depths. Therefore, we have established that the GEM-3 is capable of delivering broadband EMI data with ample target-specific information for the purpose of target classification and identification.

Appendix G

Paper to be presented at the Annual Symposium on the Application of Geophysics to Engineering and Environmental Problems (SAGEEP), 20-24, February, 2000, Arlington, Virginia.

CHARACTERIZATION STUDIES OF THE ELECTROMAGNETIC INDUCTION RESPONSE OF COMPACT METALLIC OBJECTS FOR IMPROVED UNEXPLODED ORDNANCE / CLUTTER DISCRIMINATION

B. Barrow, T. Bell, and J. Miller.

Annual Symposium on the Application of Geophysics to Engineering and Environmental Problems (SAGEEP)
Of the Environmental and Engineering Geophysical Society (EEGS), 20-24 February 2000,
Arlington, Virginia,

CHARACTERIZATION STUDIES OF THE ELECTROMAGNETIC INDUCTION RESPONSE OF COMPACT METALLIC OBJECTS FOR IMPROVED UNEXPLODED ORDNANCE / CLUTTER DISCRIMINATION

Bruce Barrow, Thomas H. Bell, and Jonathan Miller
AETC, Inc.
1225 Jefferson Davis Highway, Suite 800, Arlington, VA 22202
(703) 413-0500 • fax (703) 413-0512 • bjb@va.aetc.com

ABSTRACT

A simple induced dipole model has been found to effectively fit a large collection of measured data over many compact metallic objects using several different types of EMI sensors. The induced moment is determined by a set of response coefficients that depend on the object's size, shape, and material properties. To the extent that these response coefficients differ between ordnance and clutter, discrimination using EMI sensors may be possible. Observed differences in the relative strength of these coefficients between flat and long objects have already been applied as a means of shape discrimination. Presently, these coefficients are determined by direct measurement with a given EMI sensor. In an effort to empirically understand how these coefficients depend on the object, careful measurements have been made as a function of frequency over simple shapes like spheres and cylinders. A baseline model has been found that fits most of the data, even UXO and clutter. To first order, the model parameters can be related to physical parameters. For ferrous cylinders, the frequency response curves can be scaled to cylinder diameter and aspect ratio. From this baseline model, future measurements will try to understand the effects of tapering the cylinders to UXO-like shapes and then the effects of adding fins and driving bands.

INTRODUCTION

Currently, most unexploded ordnance (UXO) remediation is carried out with magnetic and electromagnetic induction (EMI) sensors. While highly effective in detecting metallic objects such as UXO, present field techniques also result in many false targets from other metallic scrap (Office of the Undersecretary of Defense, 1997). To reduce the cost of digging non-UXO, discrimination techniques using both current and future EMI technologies are needed.

A large quantity of controlled EMI data has been collected recently under a variety of programs (Burr, 1999; UXOCOE, 1999). A number of sensors have been tested: the Geonics EM61, the Geonics EM61HH, the Geophex GEM-3, the Minelab F1A4-D, and the U.S. Army AN/PSS12. Most of these are time domain (TD) sensors with only one or two time gates. The GEM-3 is a frequency domain sensor with a range from 30 Hz to 24 kHz. Objects buried for these tests have included UXO ranging from 20mm projectiles to 155mm shells. Clutter objects have included pipes, plates, nails, cans, a shovel blade, a fence post cap and other assorted scrap. For most of this data and all of these sensors, the data can be empirically modeled as an induced dipole response in the object. The magnitude and direction of this dipole moment is determined by the

field at the object from the transmitter, the direction of this field relative to the major physical axes of the object, and empirically determined response coefficients along these physical axes. The voltage induced in the receiver coil(s) by this dipole moment then determines the sensor response.

For a given object, the response coefficients are a function of the time gate(s) or frequencies used by the EMI sensor. It is the relative magnitude and functional dependence on time/frequency of these coefficients that drive the problem of discriminating UXO from clutter. These coefficients are determined by the physical properties of the object: size, shape, magnetic permeability, and electrical conductivity. If they do not vary significantly between a given UXO item and a common clutter item then it will not be possible to discriminate between these with any EMI sensor. If the response coefficients are not different over a narrow range of frequencies or a narrow range of time gates, then an EMI sensor operating in this range will not provide any discrimination capability.

In an effort to understand how these coefficients scale with the object's physical parameters, we have been making controlled measurements with the GEM-3 starting with very simple shapes: spheres and cylinders. After careful calibration of the GEM-3, the measurements made on spheres match the expected analytic solution very well (Miller, et al, these proceedings). By comparing the analytic solutions for spheres and infinite cylinders to the measured response of ferrous cylinders of varying size and aspect ratio, a simple functional form was found for the response coefficients of cylinders as a function of frequency. In turn, it was found that this simple function could be fit to the response of a wide variety of ordnance and clutter.

In the next section, the basic idea of the induced dipole response model will be presented. Examples will be shown with three basic EMI sensors over several different types of ordnance. Following this, the functional form of the response coefficients as a function of frequency will be discussed. Examples will be shown for a variety of objects. For ferrous cylinders of a fixed aspect ratio, the response curves fit to a single functional form, when the model is scaled appropriately. In the conclusion, we will discuss ways that these results are being applied and what future work will be done.

INDUCED DIPOLE RESPONSE MODEL

Modeling the response of an object to an EMI sensor as an induced dipole moment has been found to work for a variety of instruments and objects. This dipole moment vector, $\mathbf{m}$, can be expressed as:

$$\mathbf{m}(\mathbf{x}_t) = \mathbf{U}\mathbf{B}\mathbf{U}^{\mathrm{T}}\mathbf{H}_0(\mathbf{x}_s, \mathbf{x}_t),$$

where $\mathbf{x}_t$ is the object location, $\mathbf{x}_s$ is the sensor location, and $\mathbf{H}_0$ is the peak magnetic field at the object from the sensor. The elements of the tensor U are the directional cosines between the coordinate directions and the principal axes of the object. The matrix B is the diagnolized matrix of response coefficients:

$$\mathbf{B} = \begin{bmatrix} \beta_x & 0 & 0 \\ 0 & \beta_y & 0 \\ 0 & 0 & \beta_z \end{bmatrix}.$$

These β coefficients are essentially a measure of how strong an object responds along each of its principal axes to a given driving field. For axisymmetric objects such as cylinders, disks, and most UXO, there are only two unique β's: β_l along the symmetry axis and β_t along two axes transverse to the symmetry axis. For TD sensors, the coefficients are a function of the driving field pulse and the time gate(s) used. For FD sensors, the coefficients are a function of the driving field frequency and are generally complex; i.e. the dipole response is phase shifted relative to the driving field. The actual values are determined by properties of the object: size, shape, magnetic permeability and electrical conductivity. The final sensor response is then determined by the voltage induced in the sensor receiver coil(s) by the time rate of change of the dipole response field from the object. This model is limited in that it assumes a uniform driving field across the object and that the object responds as a point source. But for the range of coil sizes in current EMI sensors and the range of UXO sizes and depths, the model appears to be sufficiently robust despite these assumptions.
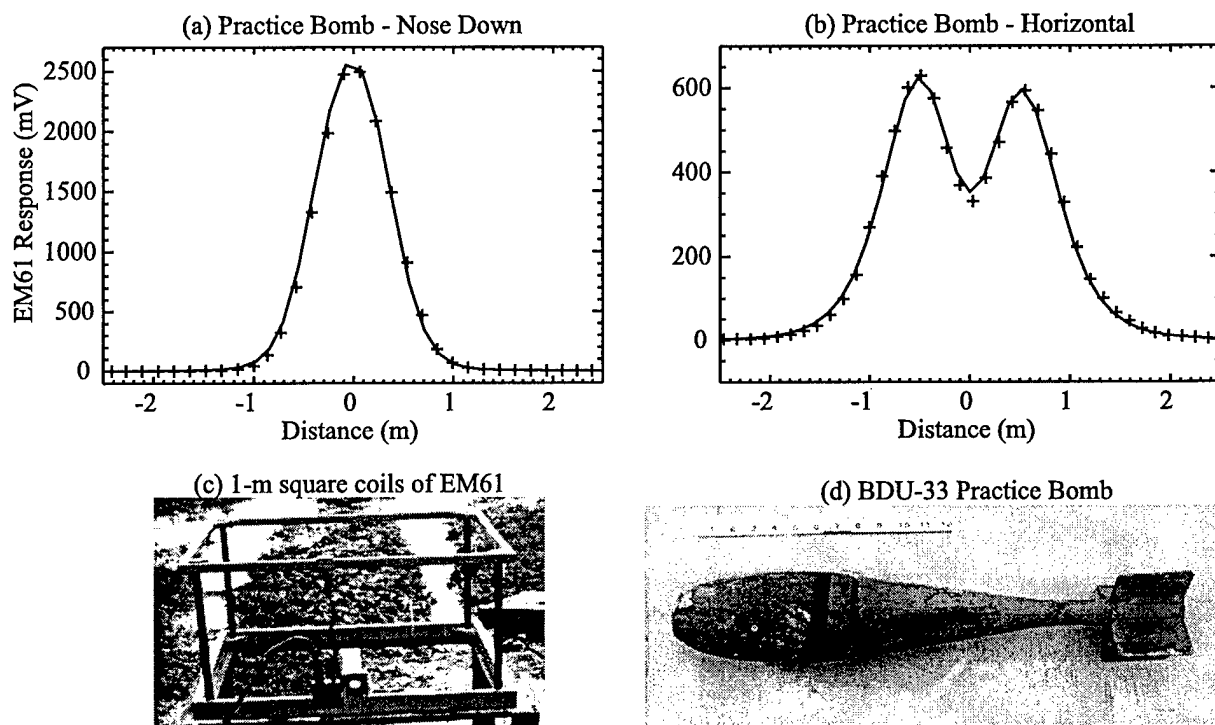
Figure 1. Measured response of an EM61 to (a) a vertical and (b) a horizontal BDU-33 practice bomb. Both cases are 0.65 m below the sensor. Symbols represent data and the line is the best induced dipole model fit to the data.

EM61 Example

Figure 1 shows the result of applying this model to an array of Geonics EM61's over a BDU-33 practice bomb. This data was collected by the Multisensor Towed Array Detection System (*MTADS*) which is a project run by the Naval Research Laboratory (McDonald and Robertson, 1996). This EMI sensor platform consists of three overlapping EM61 sensors that have an earlier time gate than the standard EM61. The EM61 consists of a one-meter square transmitter coil

with two receiver coils the same size: one is co-located with the transmitter and one is 0.4 m above this. The sensor response of the upper receiver coil from the center EM61 of the array is plotted as a function of distance as the array travels directly over the practice bomb. The symbols denote the measured values and the solid line is the best model fit to the data. In figure 1a, the bomb is oriented nose down and the midpoint of the bomb is 0.65 m below the EM61. In arbitrary units that result in standard EM61 output (milli-volts), the model response coefficients fit to $\beta_l = 7.6$ along the length of the bomb and $\beta_t = 1.4$ across its width with a ratio of $\beta_l / \beta_t = 5.4$. In figure 1b, the bomb is horizontal and laying along the direction that the EM61 array is moving. In this case, the best model fit resulted in $\beta_l = 6.6$, $\beta_t = 1.1$, and a ratio of 6.0. A response ratio greater than one is indicative of elongated ferrous objects. For spheres this ratio is one, and for flattened objects, it is less than one. How this response ratio couples between the sensor coils and the object's orientation results in very different spatial signatures for the same object. The strongest field from the transmitter coil occurs when the sensor is directly over the object. This field is vertical, and in figure 1a, couples with the strongest β. In figure 1b, the field couples with the weakest β directly over the object. However, when the coils are off to the side, the field has a strong horizontal component and then it couples well with the larger β. The result is the double peaked response. For a single time gate EMI sensor, the ratio of β's provides a way to do simple shape based discrimination between UXO and clutter. A large set of UXO is elongated and presumably some set of clutter will be roughly flat. This technique was used with reasonable success by *MTADS* at the Jefferson Proving Ground Phase IV tests and is part of a current ESTCP project with *MTADS* (Barrow and Nelson, 1999).

EM61HH Example

Figure 2 plots the results of modeling the EM61HH response to a 2.75-inch rocket warhead. The EM61HH consists of two circular coils, each about 17 cm in diameter. The two circular coils are laying flat and their centers are separated by 13 cm. The EM61HH has two time gates instead of the two receiver coils of the EM61. The first time gate is roughly 0.16 milli-seconds after the pulse and the second is 0.6 milli-seconds after. Typically, the coils are on wheels with one coil leading the other. The warhead is lying flat along this direction. Figure 2a and 2b plot the early and late time gates respectively. The symbols are the measured results and the lines are the best model fits. The plus symbols and the solid line denote measurements as the sensor moves along the length of the object in its typical fashion. The triangle symbols and dotted lines are the result if the sensor is moved left to right over the object, but with one coil still leading the other in a forward fashion. In units to match EM61HH output, the relative β values are: $\beta_l = 1.7$, $\beta_t = 0.7$, and a ratio of 2.4 for the first time gate. For the second time gate, they are: $\beta_l = 0.43$, $\beta_t = 0.1$, and a ratio of 4.3. The ratio of the β values is larger for the late time gate, and the double peaked structure is more pronounced because of this. Figure 2c plots the β values as a function of time after the pulse. The magnitudes are decaying as expected, but at different rates for β_l (solid line) and β_t (dashed line). Ideally, one would like to measure the shape of these decay curves with enough time gates to provide optimal discrimination between UXO and clutter. Geonics is said to be working on a multiple time gate EMI sensor.
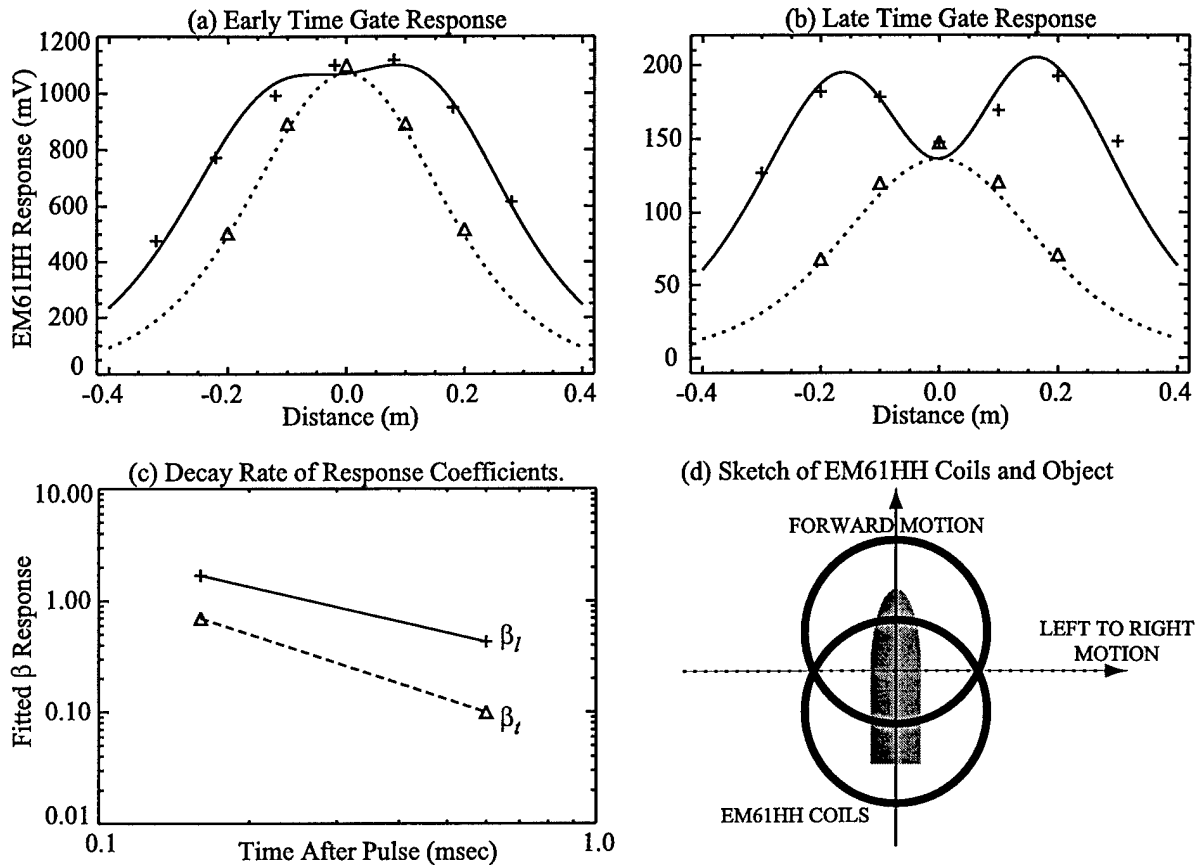
Figure 2. Measured response of EM61HH over a horizontal 2.75" rocket warhead. Plus symbols are data points as sensor moves in forward fashion over object and solid line is the best model fit. Triangles are measured data as sensor is moved left to right over object and dotted line is best model fit. Plots (a) and (b) represent the early (0.16 msec) and late (0.6 msec) time gates, respectively. Plot (c) shows the decay rates for the two model response coefficients.

GEM-3 Example

The GEM-3 is a FD sensor with a driving frequency that goes from 30 Hz to 24 kHz. It consists of a circular driving coil that is 52 cm in diameter and a circular receiver coil centered in this that is 8 cm in diameter. Because the driving field is always on, there is a 32-cm bucking coil to cancel the driving field at the location of the receiver. The GEM-3 measures the inphase and quadrature (90 degrees out of phase) response from an object. Figure 3 plots the measured responses at 270 Hz (3a) and at 24kHz (3b) from a 30mm projectile (25 cm below the coil, lying horizontal along the direction of travel). The symbols are the measured data (plus-inphase, triangle-quadrature), and the lines are model fits (solid-inphase, dotted-quadrature). Figure 3c plots the fitted β's as a function of frequency (solid-inphase, dotted-quadrature). At 270 Hz, the β_l/β_t ratios are 1.8 inphase and 4.8 quadrature. Again at large values for the ratio, a double peak is observed. At 24 kHz, the ratios are 1.0 inphase and 0.85 quadrature. For the quadrature response, the ratio has actually gone from much greater than one to less than one. These frequency dependent curves of the response coefficients have very different relative magnitudes
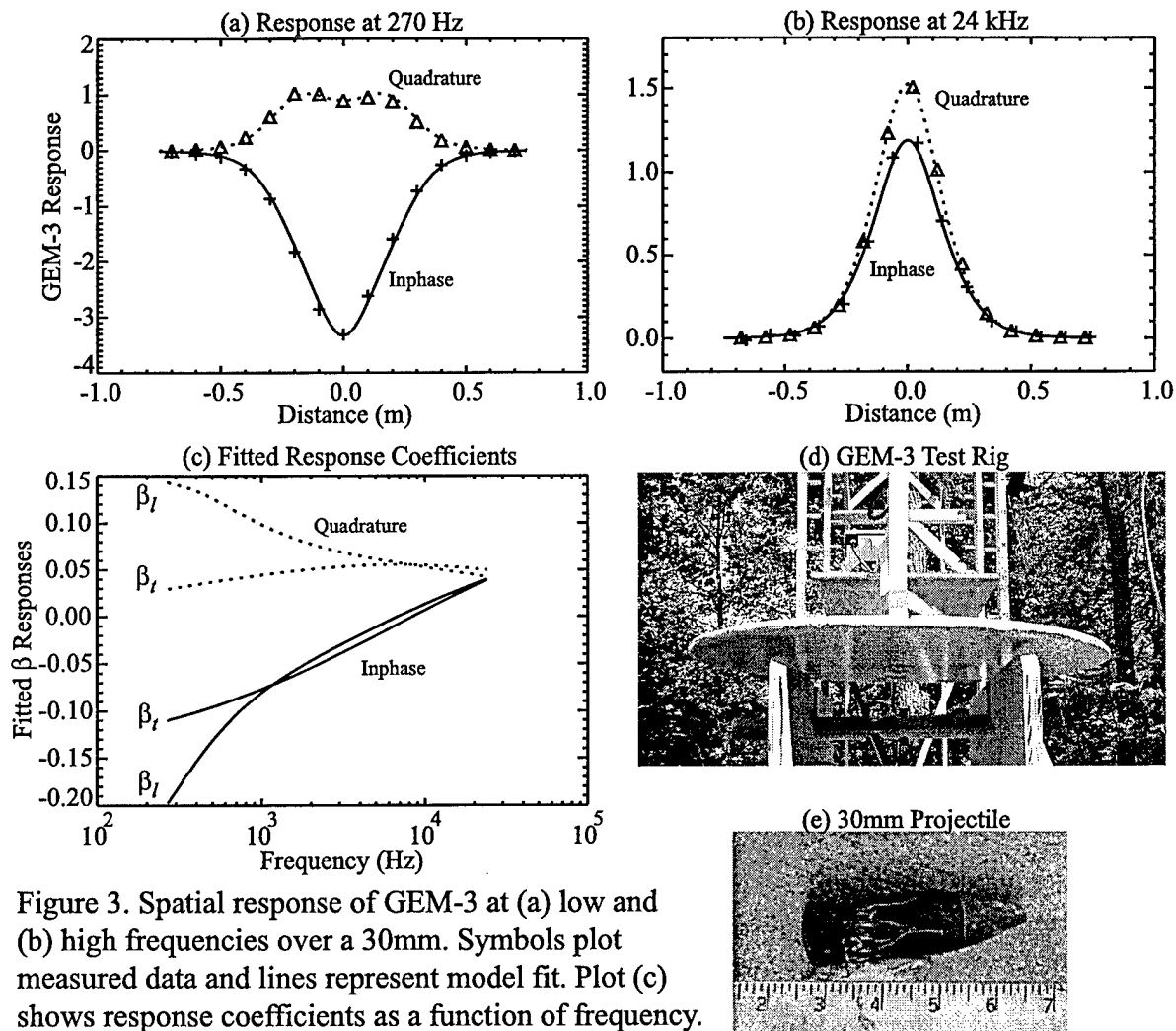
Figure 3. Spatial response of GEM-3 at (a) low and (b) high frequencies over a 30mm. Symbols plot measured data and lines represent model fit. Plot (c) shows response coefficients as a function of frequency.

and shapes. An EMI sensor that can collect this data over an appropriate range of frequencies (or time gates) will provide the best discrimination between UXO and clutter.

CONTROLLED MEASUREMENTS OF RESPONSE COEFFICIENTS

Analytic solutions exist for the induced dipole moment of a sphere (Grant and West, 1965) and an infinite cylinder (Ward and Hohmann, 1987) in a spatially uniform, harmonically time varying field. In the case of the sphere, the solution is:

$$\mathbf{m} = -2\pi a^3 (X + iY)\mathbf{H}_0,$$

where a is the sphere radius, $\mathbf{H_0}$ is the primary field, and $X+iY$ is a set of complex response functions for each value of μ that scales with the dimensionless parameter $k^2 a^2 = \sigma\mu\omega a^2$. This scaling parameter is essentially the frequency of the driving field, $f = \omega / 2\pi$, multiplied by a diffusion time constant, $\tau = \sigma\mu a^2$, where σ is the electrical conductivity and μ is the magnetic permeability of the sphere. Measurements made with the GEM-3 on metal spheres have been

found to match this analytic solution very well (Miller et al, these proceedings). The solution for an infinite cylinder has a similar form with a different set of complex response functions, $X+iY$. It was observed that in the limit of highly permeable objects, $\mu/\mu_0 > 10$, that the cylinder response function is essentially, 2/3*(sphere solution) + 1/3.

From this observation and data measured by the GEM, a baseline model for all response functions was developed where the general form is just $a*(X+iY)+b$, where $X+iY$ is the response function of a sphere. The constant a determines the range of the response function from high to low frequency relative to the sphere solution. The constant b determines the high frequency limit relative to the sphere limit multiplied by a. Effectively, these two constants are just stretching and shifting the sphere's response function. For uniformly magnetized objects, the low and high frequency limits of the response function can be shown to be a function of μ and a demagnetization factor, n (Bell et al, 1998). The end result is a three parameter fit (μ, n, and σ) that appears to fit the measured response curves of a variety of objects. Figure 4 plots the results of these fits for six different objects: a 3" chrome steel sphere, a 1" by 4" steel cylinder, a square steel plate, a piece of I bar, a 60mm mortar, and a 37mm projectile. Curiously, it is an ordnance item that shows the largest deviation from this baseline model.

While this three-parameter model fits most of the data, it is not clear to what extent the fit parameters reflect the object's true physical properties. This is particularly true of the demagnetization factor, which is typically defined in terms of a uniformly magnetized object. For objects with sharp edges and objects in a non-uniform field, this may not be a good assumption. In an effort to understand how these "effective" fit parameters are actually scaling with true physical parameters, a large number of ferrous circular cylinders have been measured with the GEM sensor. Diameters from 0.25 to 6 inches and aspect ratios (length to diameter) of 2, 4, and 8 have been measured. The cylinders were measured in two orientations: vertical and horizontal directly under the sensor coils and placed at a range of distances. For each set of fixed aspect ratio cylinders in a given orientation, it was found that all of the data could be fit to single response curve if an extra amplitude scaling factor were allowed for each measurement. Figure 5 illustrates this for the set of aspect ratio 4 cylinders oriented vertically under the GEM sensor; similar curves have been produced for aspect ratios of 2, 4, and 8 oriented both vertically and horizontally. The fit parameters of $\mu/\mu_0 = 13.1$, $\sigma = 3.1 \times 10^7$ mho/m, and $n = 0.0103$ resulted in the solid line shown. The actual measurements are plotted as various symbols for each cylinder. The added amplitude factor was roughly constant as a function of distance for some cylinders and changed for others. The demagnetization factor is within the range of published values, but not equal considering various sources of error.

CONCLUSIONS

For a range of EMI sensors both FD and TD, the response of compact metallic objects can be modeled as an induced dipole moment. This induced moment is determined by response coefficients that are unique to an object's physical parameters such as size and shape. These response coefficients are a function of the frequencies or time gates used by the EMI sensor, and currently, are determined empirically by measuring the object with a given sensor. The relative magnitudes of these coefficients along the physical axes of an object are an indicator of an
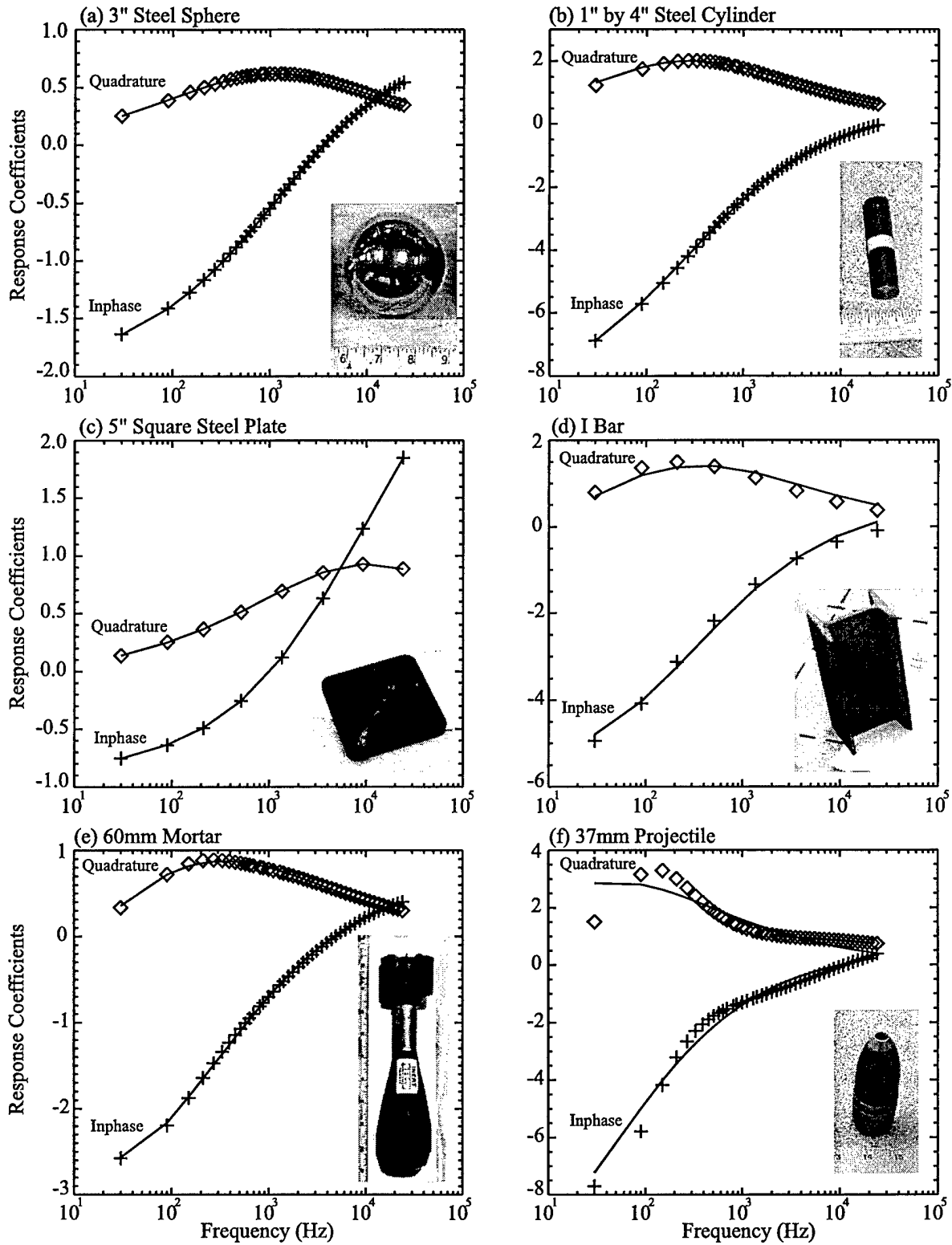
Figure 4. Inphase (plus) and quadrature (diamond) response of GEM-3 to a variety of objects. Lines represent three parameter model fit to response as a function of frequency.

Response Function, $X + iY$

0

-5

-10

-15

-20

— — 0.25" diameter - 5 depths.
← — 0.50" diameter - 7 depths.
▲ — 1.00" diameter - 8 depths.
— ·— 2.00" diameter 12 depths.
← ·— 4.00" diameter - 14 depths.
▲ ·— 6.00" diameter - 12 depths.
—— BASELINE MODEL

$\mu / \mu_0 = 13.1$ (all data)
$\sigma = 3.1\,E\,7$ mho/m (all data)
Demagnetization factor = 0.0103

Amplitudes of each response
adjusted to match model.

1   10   100   1000
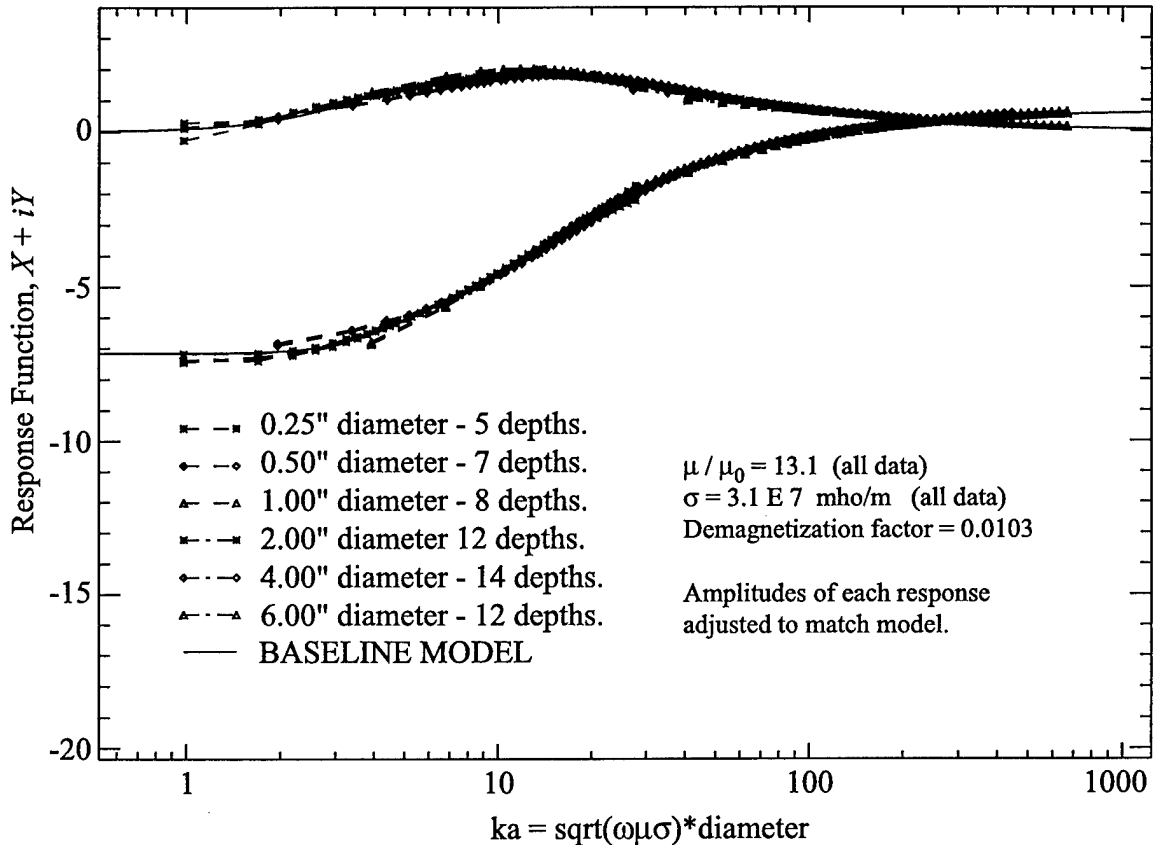
$ka = sqrt(\omega\mu\sigma)*diameter$

Figure 5. Response curves for all vertical, aspect ratio 4 cylinders and best common fit to three parameter baseline model.

object's shape. Using this model, it is a relatively simple matter to develop algorithms to invert EMI data over an unknown object and estimate its response coefficients and physical orientation. It has been observed that the accuracy of this inversion is limited by the measured data. The difference in signals from a particular ordnance item and a rectangular metal plate can be very small and the data measured over each must be spatially dense and accurately mapped for the inverted model parameters to accurately resolve the two objects (Barrow and Nelson, 1999).

Because these response coefficients result from the physical parameters of the object, it is important to understand how they scale with size, shape, material properties, and the frequency / time gate of the EMI sensor. It is the differences in these coefficients that limit how well all EMI sensors can discriminate between UXO and common metallic clutter. As a first step towards understanding these coefficients in the frequency domain, a large number of both simple (spheres and cylinders) and complex objects (UXO and clutter) have been carefully measured with the GEM-3. Almost all of the items have been found to fit a simple three-parameter model. We are beginning to understand how the fit parameters scale for ferrous cylinders of different sizes and aspect ratios. We are presently attempting to numerically model the high and low frequency limits of cylinders in non-uniform driving fields (like the GEM-3) to explain our observations. Concurrently with this modeling effort, we are modifying the basic cylinders to see how the baseline response curves change. The first step is to taper one end of the cylinder to make it

resemble ordnance. The effects of fins and driving bands are also being considered. Presently, ordnance items with intact driving bands, like the 37mm in fig 4f, show the largest deviation from the baseline model (more than any clutter item). Lastly, as time domain measurements become available, it is a simple matter to convolve these frequency response curves with the sensor driving pulse in the fourier domain to predict what the time gate decay curves will be. For either type of EMI sensor, optimal ranges of frequencies or time gates may provide the best possible discrimination.

ACKNOWLEDGMENTS

REFERENCES

Barrow, B., and Nelson, H.H., "Model-Based Characterization of EM Induction Signatures for UXO/Clutter Discrimination Using the *MTADS* Platform," Proceedings of UXO Forum, 1999.

Bell, T.H., et al, "Shape-Based Classification and Discrimination of Subsurface Objects Using Electromagnetic Induction," International Geoscience and Remote Sensing Symposium, 1998.

Burr, A. P., "Phase IV Advanced Technology Demonstrations at Jefferson Proving Ground," UXO Forum, 1999.

Grant, F., and West, G., *Interpretation Theory in Applied Geophysics*, McGraw-Hill Book Co., New York, pp 492, 1965.

McDonald, J. R., and Robertson, R., "Multi-Sensor Towed Array Detection System," Proceedings of UXO Forum '96, pp. 53-59, March 1996.

Miller, J., et al, "Electromagnetic Induction Response of Spherical Conductors Measured with the GEM-3 Sensor and Compared to Analytic Models," these proceedings.

Office of the Undersecretary of Defense (Acquisition and Technology), "Report to Congress: Unexploded Ordnance Clearance," pp. 25-26, March 1997.

UXO Center of Excellence (UXOCOE), "Unexploded Ordnance Detection and Clearance Technology Development," http://www.denix.osd.mil/UXOCOE, 1999.

Ward, S. H., and Hohmann, G. W., "Electromagnetic Theory for Geophysical Applications," pp258. *Electromagnetic Methods in Applied Geophysics*, Society of Exploration Geophysicists, 1987.

Appendix H

PROCESSING TECHNIQUES FOR DISCRIMINATION BETWEEN BURIED
UNEXPLODED ORDNANCE AND CLUTTER USING MULTISENSOR ARRAY DATA

T. Bell, J. Miller, D. Keiswetter, B. Barrow, and I. J. Won.

Processing Techniques for Discrimination Between Buried Unexploded Ordnance and Clutter Using Multisensor Array Data

THOMAS H. BELL

AETC Incorporated,

1225 Jefferson Davis Highway, Suite 800

Arlington, VA 22202

(703) 413-0500

tbell@va.aetc.com

Co-Performers: Jonathan Miller, Dean Keiswetter, Bruce Barrow, I.J. Won

This project addresses the issue of discriminating between buried unexploded ordnance (UXO) and clutter in the context of environmental cleanup. In spite of the recent advances in UXO detection performance, false alarms due to clutter (signals incorrectly diagnosed as having been caused by UXO) remain a serious problem. With traditional survey methods, the Army Corps of Engineers finds that 85-95% of all detected targets are not UXO. Since the cost of identifying and disposing of UXO in the United States using current technologies is estimated to range up to $500 billion, increases in performance efficiency due to reduced false alarm rates can result in substantial cost savings.

Typical ordnance items have certain distinctive attributes that distinguish them from clutter. They have a characteristic shape (long and slender) and their composition is distinctive (typically comprising a steel body with a brass or aluminum fuze body and copper driving bands or an aluminum fin assembly). Our experience is that these attributes correspond to distinctive signatures in magnetic and electromagnetic induction sensor data. Current research activities are directed towards exploiting differences in shape between ordnance and clutter with commercially available sensors. In this project we systematically explore the performance improvements which are realized when additional distinguishing target attributes are included in the discrimination process. The technical objective is to develop a reliable technique for discriminating between buried UXO and clutter using multisensor electromagnetic induction sensor array data.

During the first year we have developed a baseline model for the EMI signatures of simple slender objects (rods), and have established that the EMI signatures of ordnance items of comparable size and length-to-diameter aspect ratio differ in significant ways from the baseline.

Appendix I

Abstract accepted for an oral presentation at the UXO / Countermine Forum, May 2-4, 2000, Anaheim, California

DETECTION OF COPPER ROTATING BANDS ON BURIED ORDNANCE USING WIDE-BAND ELECTROMAGNETIC INDUCTION

J. Miller, T. Bell, D. Keiswetter.

DETECTION OF COPPER ROTATING BANDS ON BURIED ORDNANCE USING WIDE-BAND ELECTROMAGNETIC INDUCTION

Jonathan Miller*, Thomas Bell
AETC,Inc
1225 Jefferson Davis Highway, Suite 800
Arlington, VA 22202
jtmiller@va.aetc.com
phone•(703) 413-0500 *fax*•(703) 413-0512
*Presenter/Point of Contact

Dean Keiswetter
Geophex, Ltd.
605 Mercury St.
Raleigh, NC 27603
keiswetter@geophex.com
phone•(919) 839-8515 *fax*•(919) 839-8528

***Abstract Category:* DETECTION**

Rotating bands are soft metal rings near the tail of a projectile designed to make sliding contact with rifling grooves in the gun bore when the projectile is fired. They are typically made of copper and found on a wide variety of projectile types and sizes. In this paper we demonstrate that rotating bands are particularly easy to detect and identify using wide band electromagnetic induction (EMI) instrumentation. Our finding is supported by a large set of data collected on a variety of objects under both controlled conditions and in the field. Rotating bands contribute a strong and distinctive signal to the overall response of an ordnance item, characterized by a relatively sharp peak in quadrature, similar to the response of a wire loop alone. We attribute this signal to a combination of three factors: 1) the relatively high conductivity of rotating bands compared with the body of the projectile, 2) the fact that rotating bands are in the shape of a loop, and 3) the capability of wide-band EMI instruments to sweep a range of frequencies, ensuring excitation of the frequencies where the rotating band contribution is strong. We find that the frequency of the quadrature peak is related to the diameter of the rotating band, which suggests this signal may be very useful in identifying targets.